Draft version April 30, 2026
Typeset using LaTeX **twocolumn** style in AASTeX631

Searches for Binary Mergers with Sub-solar Mass Components in Data from the First Part of LIGO–Virgo–KAGRA's Fourth Observing Run

A. G. Abac,[1] I. Abouelfettouh,[2] F. Acernese,[3,4] K. Ackley,[5] A. Adam,[6] C. Adamcewicz,[7] S. Adhicary,[8] D. Adhikari,[9,10] N. Adhikari,[11] R. X. Adhikari,[12] V. K. Adkins,[13] S. Afroz,[14] A. Agapito,[15] D. Agarwal,[16] M. Agathos,[17] N. Aggarwal,[18] S. Aggarwal,[19] O. D. Aguiar,[20] I.-L. Ahrend,[21] L. Aiello,[22,23] A. Ain,[24] P. Ajith,[25] T. Akutsu,[26,27] S. Albanesi,[28,29] L. Albers,[30] W. Ali,[31,32] S. Al-Kershi,[9,10] C. Alléné,[33] A. Allocca,[34,4] S. Al-Shammari,[35] P. A. Altin,[36] S. Alvarez-Lopez,[37] W. Amar,[33] O. Amarasinghe,[35] A. Amato,[38,39] F. Amicucci,[40,41] C. Amra,[42] C. Anand,[7] A. Ananyeva,[12] S. B. Anderson,[12] W. G. Anderson,[12] M. Andia,[43] M. Ando,[44,45] M. Andrés-Carcasona,[37] J. L. Andrey,[46] T. Andrić,[47,48] J. Anglin,[49] J. Anna,[50] S. Ansoldi,[51,52] J. M. Antelis,[53] S. Antier,[43] M. Aoumi,[54] E. Z. Appavuravther,[55,56] S. Appert,[12] S. K. Apple,[57] K. Arai,[12] A. Araya,[58] M. C. Araya,[12] M. Arca Sedda,[47,48] F. Arciprete,[22,23] J. S. Areeda,[59] N. Aritomi,[2] F. Armato,[31,32] S. Armstrong,[60] N. Arnaud,[61] M. Arogeti,[62] S. M. Aronson,[49] G. Ashton,[63] Y. Aso,[54,64] L. Asprea,[29] M. Assiduo,[65,66] S. Assis de Souza Melo,[67] S. M. Aston,[68] P. Astone,[40] F. Attadio,[41,40] F. Aubin,[69] K. AultONeal,[50] G. Avallone,[70] E. A. Avila,[53] S. Babak,[21] C. Badger,[71] S. Bae,[72] S. Bagnasco,[29] L. Baiotti,[73] R. Bajpai,[74] T. Baka,[75,39] K. A. Baker,[6] T. Baker,[76] G. Balbi,[77] G. Baldi,[78,79] N. Baldicchi,[80,55] M. Ball,[81] G. Ballardin,[67] S. W. Ballmer,[82] S. Banagiri,[7] B. Banerjee,[47] D. Bankar,[83] T. M. Baptiste,[13] P. Baral,[11] M. Baratti,[84,85] J. C. Barayoga,[12] K. Baric,[12] B. C. Barish,[12] D. Barker,[2] N. Barman,[83] P. Barneo,[86,87,88] F. Barone,[89,4] B. Barr,[90] M. Barrios,[91] L. Barsotti,[37] M. Barsuglia,[21] D. Barta,[92] M. A. Barton,[90] I. Bartos,[49] A. Basalaev,[9,10] R. Bassiri,[93] A. Basti,[85,84] M. Bawaj,[80,55] P. Baxi,[94] J. C. Bayley,[90] A. C. Baylor,[11] P. A. Baynard II,[62] M. Bazzan,[95,96] V. M. Bedakihale,[97] F. Beirnaert,[98] M. Bejger,[99] D. Belardinelli,[23] A. S. Bell,[90] C. Bellani,[100] L. Bellizzi,[84,85] D. Beltran-Martinez,[101] W. Benoit,[19] I. Bentara,[61] M. Ben Yaala,[60] S. Bera,[102] F. Bergamin,[35] B. K. Berger,[93] S. Bernuzzi,[28] M. Beroiz,[12] C. P. L. Berry,[90] I. Berry,[103] D. Bersanetti,[31] T. Bertheas,[104] A. Bertolini,[39,38] J. Betzwieser,[68] D. Beveridge,[6] G. Bevilacqua,[105] N. Bevins,[106] R. Bhandare,[107] R. Bhatt,[12] A. Bhattacharjee,[108] D. Bhattacharjee,[109,110] S. Bhattacharyya,[111] S. Bhaumik,[49] V. Biancalana,[105] A. Bianchi,[39,112] F. Bianchi,[55] I. A. Bilenko,[113] G. Billingsley,[12] A. Binetti,[100] S. Bini,[78,79,12] C. Binu,[114] S. Biot,[115] O. Birnholtz,[116] S. Biscoveanu,[117] A. Bisht,[10] M. Bitossi,[67,84] M.-A. Bizouard,[118] S. Blaber,[119] J. K. Blackburn,[12] L. A. Blagg,[81] C. D. Blair,[6,68] D. G. Blair,[6] N. Bode,[9,10] N. Boettner,[30] P. Bogdan,[120] G. Boileau,[118] M. Boldrini,[40] G. N. Bolingbroke,[121] A. Bolliand,[122,42] L. D. Bonavena,[49] R. Bondarescu,[86] F. Bondu,[123] V. A. Bonhomme,[37] E. Bonilla,[93] M. S. Bonilla,[59] A. Bonino,[124] R. Bonnand,[33,122] A. Borchers,[9,10] N. Borghi,[125,77] V. Boschi,[84] S. Bose,[126] V. Bossilkov,[68] Y. Bothra,[39,112] A. Boudon,[61] M. Boyle,[127] A. Bozzi,[67] C. Bradaschia,[84] M. J. Brady,[128] P. R. Brady,[11] A. Branch,[68] M. Branchesi,[47,48] T. Briant,[129] A. Brillet,[118] M. Brinkmann,[9,10] P. Brockill,[11] E. Brockmueller,[9,10] A. F. Brooks,[12] B. C. Brown,[49] D. D. Brown,[121] M. L. Brozzetti,[80,55] S. Brunett,[12] G. Bruno,[16] R. Bruntz,[120] J. Bryant,[124] Y. Bu,[130] F. Bucci,[66] J. Buchanan,[120] O. Bulashenko,[86,87] T. Bulik,[131] H. J. Bulten,[39] A. Buonanno,[132,1] K. Burtnyk,[2] R. Buscicchio,[133,134] D. Buskulic,[33] C. Buy,[104] R. L. Byer,[93] R. Cabrita,[16] V. Cáceres-Barbosa,[8] L. Cadonati,[62] G. Cagnoli,[135] C. Cahillane,[82] A. Calafat,[136] T. A. Callister,[137] E. Calloni,[34,4] S. R. Callos,[81] G. Caneva Santoro,[138] K. C. Cannon,[45] H. Cao,[37] L. A. Capistran,[139] E. Capocasa,[21] G. Capoccia,[55] E. Capote,[2] G. Capurri,[85,84] G. Carapella,[70,140] F. Carbognani,[67] K. J. Cardona-Martínez,[13] M. Carlassara,[9,10] J. B. Carlin,[130] T. K. Carlson,[141] M. F. Carney,[109] M. Carpinelli,[133,67] G. Carrillo,[81] J. J. Carter,[9,10] G. Carullo,[124] A. Casallas-Lagos,[142] J. Casanueva Diaz,[67] C. Casentini,[143,23] S. Caudill,[141] M. Cavaglià,[110] R. Cavalieri,[67] G. Cella,[84] S. Cepic,[125] P. Cerdá-Durán,[144,145] E. Cesarini,[23] N. Chabbra,[36] W. Chaibi,[118] A. Chakraborty,[14] P. Chakraborty,[9,10] S. Chakraborty,[107] S. Chalathadka Subrahmanya,[30] R. Chalmers,[76] C. Chan,[146] J. C. L. Chan,[147] M. Chan,[119] K. Chang,[148] P. Charlton,[149] E. Chassande-Mottin,[21] C. Chatterjee,[150] Debarati Chatterjee,[83] Deep Chatterjee,[37] M. Chaturvedi,[107] S. Chaty,[21] A. Chen,[151] A. H.-Y. Chen,[152] D. Chen,[153] H. Chen,[154] H. Y. Chen,[155] S. Chen,[150] Y. Chen,[156] G. Cheng,[151] H. P. Cheng,[103] P. Chessa,[80,55] T. Cheunchitra,[130] H. T. Cheung,[94] S. Y. Cheung,[7] F. Chiadini,[157,140] G. Chiarini,[9,10] A. Chiba,[158] A. Chincarini,[31] D. Chintala,[109] M. L. Chiofalo,[85,84] A. Chiummo,[4,67] C. Chou,[159] S. Choudhary,[6] N. Christensen,[118,160] S. S. Y. Chua,[36] G. Ciani,[78,79] P. Ciecielag,[99] M. Cieślar,[131] M. Cifaldi,[23] B. Cirok,[161] F. Clara,[2] J. A. Clark,[12,62] T. A. Clarke,[7] P. Clearwater,[146] S. Clesse,[115] F. Cleva,[118] S. M. Clyne,[128] E. Coccia,[47,48,138] E. Codazzo,[162] P.-F. Cohadon,[129] D. E. Cohen,[9,10] S. Colace,[32] E. Colangeli,[76] O. Cole,[146] M. Colleoni,[136] C. G. Collette,[163] J. Collins,[68] S. Colloms,[90] A. Colombo,[164,134] C. M. Compton,[2] G. Connolly,[81] L. Conti,[96] T. R. Corbitt,[13] I. Cordero-Carrión,[165] S. Corezzi,[80,55] N. J. Cornish,[166] I. Coronado,[167] A. Corsi,[168] L. A. Corubolo,[22,23] L. Cotnoir,[120] R. Cottingham,[68] M. W. Coughlin,[19] P. Couvares,[12,62] D. M. Coward,[6] D. C. Coyne,[12] R. Coyne,[128] A. Cozzumbo,[47] J. D. E. Creighton,[11] T. D. Creighton,[169] S. Crook,[68] R. Crouch,[2] J. Csizmazia,[2] J. R. Cudell,[170] T. J. Cullen,[12] A. Cumming,[90] E. Cuoco,[125,77] M. Cusinato,[144] L. V. Da Conceição,[171] T. Dal Canton,[43] S. Dall'Osso,[172,77] S. Dal Pra,[173] G. Dálya,[104] O. Dan,[116] Y. Dang,[8] B. D'Angelo,[31] S. Danilishin,[38,39] S. D'Antonio,[40] K. Danzmann,[9,10] K. E. Darroch,[120] L. P. Dartez,[68] R. Das,[111] A. Dasgupta,[97] V. Dattilo,[67] A. Daumas,[21] I. Dave,[107] A. Davenport,[174] M. Davier,[43] T. F. Davies,[6] D. Davis,[12] L. Davis,[6] M. C. Davis,[19] P. Davis,[175,176] E. J. Daw,[177] M. Dax,[1] J. De Bolle,[98] M. Deenadayalan,[83] J. Degallaix,[178] M. De Laurentis,[34,4] C. J. Delgado Mendez,[101] F. De Lillo,[24] S. Della Torre,[134] W. Del Pozzo,[85,84] O. M. del Rio,[179] A. Demagny,[33] F. De Marco,[41,40] G. Demasi,[180,66] F. De Matteis,[22,23] N. Demos,[37] T. Dent,[181] A. Depasse,[16] N. DePergola,[106] R. De Pietri,[182,183] R. De Rosa,[34,4] C. De Rossi,[67] M. Desai,[37] V. Deshmukh,[90] R. De Simone,[157,140] S. Determan,[184] A. Dhani,[1] R. Dhurkunde,[76] R. Diab,[49] C. Diaz,[101] M. C. Díaz,[169] M. Di Cesare,[34,4] G. Dideron,[185] T. Dietrich,[1] L. Di Fiore,[4] C. Di Fronzo,[6] M. Di Giovanni,[186,84] T. Di Girolamo,[34,4] D. Diksha,[39,38] J. Ding,[37,21,187] S. Di Pace,[41,40] I. Di Palma,[41,40] D. Di Piero,[188,52] F. Di Renzo,[66,180] Divyajyoti,[35] A. Dmitriev,[124] J. P. Docherty,[90] Z. Doctor,[117] N. Doerksen,[171] E. Dohmen,[2] A. Doke,[141] A. Domiciano De Souza,[189] L. D'Onofrio,[4] F. Donovan,[37] K. L. Dooley,[35] T. Dooney,[75] S. Doravari,[83] O. Dorosh,[190] F. Dosopoulou,[35] W. J. D. Doyle,[120] M. Drago,[41,40] J. C. Driggers,[2] M. Dubois,[104] R. R. Dumbreck,[35] L. Dunn,[130] U. Dupletsa,[47] D. D'Urso,[191,162] P. Dutta Roy,[49] H. Duval,[192] P.-A. Duverne,[21] S. E. Dwyer,[2] C. Eassa,[2] M. Eberhardt,[184] M. Ebersold,[193,33] T. Eckhardt,[30] G. Eddolls,[82] A. Effler,[68] J. Eichholz,[36] H. Einsle,[118] M. Eisenmann,[26] R. A. Eisenstein,[37] M. Emma,[63] K. Endo,[158] R. Enficiaud,[1] L. Errico,[34,4] R. Espinosa,[169] M. Esposito,[4,34] R. C. Essick,[194] H. Estellés,[1] T. Etzel,[12] M. Evans,[37] T. Evstafyeva,[185] B. E. Ewing,[8] J. M. Ezquiaga,[147] F. Fabrizi,[65,66] V. Fafone,[22,23] S. Fairhurst,[35] X. Fan,[151] A. M. Farah,[137] B. Farr,[81] W. M. Farr,[195,196] M. Favata,[197] M. Fays,[170] M. Fazio,[60] J. Feicht,[12] M. M. Fejer,[93] J.-N. Feldhusen,[30] E. Fenyvesi,[92,198] J. Fernandes,[199] T. Fernandes,[200,144] D. Fernando,[114] S. Ferraiuolo,[201,41,40] T. A. Ferreira,[13] M. Ferrer,[136] F. Fidecaro,[85,84] P. Figura,[99] A. Fiori,[84,85] I. Fiori,[67] M. Fishbach,[194] R. P. Fisher,[120] R. Fittipaldi,[202,140]

V. Fiumara,[203,140] R. Flaminio,[33] S. M. Fleischer,[179] L. S. Fleming,[204] E. Floden,[19] H. Fong,[119] J. A. Font,[144,145] F. Fontinele-Nunes,[19] C. Foo,[1] B. Fornal,[205] P. W. F. Forsyth,[36] K. Franceschetti,[182] A. Franco-Ordovas,[12] F. Frappez,[33] S. Frasca,[41,40] F. Frasconi,[84] J. P. Freed,[50] Z. Frei,[206] A. Freise,[39,112] O. Freitas,[200,144] R. Frey,[81] W. Frischhertz,[68] P. Fritschel,[37] V. V. Frolov,[68] M. Fuentes-Garcia,[12] S. Fujii,[207] T. Fujimori,[208] P. Fulda,[49] M. Fyffe,[68] B. Gadre,[75] J. R. Gair,[1] S. Galaudage,[189] V. Galdi,[209] R. Gamba,[8] A. Gamboa,[1] S. Gamoji,[210] A. Ganguly,[83] B. Garaventa,[31] P. García Abia,[101] J. García-Bellido,[211] C. García-Quirós,[193] J. W. Gardner,[36] S. Garg,[45] J. Gargiulo,[67] X. Garrido,[43] A. Garron,[136] F. Garufi,[34,4] P. A. Garver,[93] C. Gasbarra,[212,23] B. Gateley,[2] F. Gautier,[213] V. Gayathri,[11] T. Gayer,[82] G. Gemme,[31] A. Gennai,[84] V. Gennari,[104] J. George,[107] R. George,[155] O. Gerberding,[30] L. Gergely,[161] Archisman Ghosh,[98] Sayantan Ghosh,[199] Shaon Ghosh,[197] Shrobana Ghosh,[9,10] Suprovo Ghosh,[214] Tathagata Ghosh,[83] J. A. Giaime,[13,68] K. D. Giardina,[68] D. R. Gibson,[204] C. Gier,[60] S. Gkaitatzis,[85,84] J. Glanzer,[12] F. Glotin,[43] J. Godfrey,[81] R. V. Godley,[9,10] P. Godwin,[12] A. S. Goettel,[35] E. Goetz,[119] J. Golomb,[12] S. Gomez Lopez,[41,40] G. González,[13] P. Goodarzi,[46] S. Goode,[7] A. Goodwin-Jones,[16] M. Gosselin,[67] C. Gostiaux,[69] R. Gouaty,[33] D. W. Gould,[36] K. Govorkova,[37] A. Grado,[80,55] A. E. Granados,[19] M. Granata,[178] V. Granata,[215,140] S. Gras,[37] P. Grassia,[12] C. Gray,[2] R. Gray,[90] G. Greco,[55] A. C. Green,[39,112] L. Green,[216] S. M. Green,[76] S. R. Green,[217] A. M. Gretarsson,[50] E. M. Gretarsson,[50] H. K. Griffin,[19] D. Griffith,[12] H. L. Griggs,[62] G. Grignani,[80,55] C. Grimaud,[33] H. Grote,[35] S. Grunewald,[1] D. Guerra,[144] A. G. Guerrero,[137] D. Guetta,[218] G. M. Guidi,[65,66] T. Guidry,[2] H. K. Gulati,[97] F. Gulminelli,[175,176] A. M. Gunny,[37] H. Guo,[151] W. Guo,[6] Y. Guo,[39,38] Anuradha Gupta,[219] I. Gupta,[8] N. C. Gupta,[97] S. K. Gupta,[49] V. Gupta,[19] N. Gupte,[1] J. Gurs,[30] N. Gutierrez,[178] N. Guttman,[7] F. Guzman,[139] D. Haba,[220] M. Haberland,[1] S. Haino,[221] E. D. Hall,[37] E. Z. Hamilton,[136] G. Hammond,[90] M. Haney,[39] J. Hanks,[2] C. Hanna,[8] M. D. Hannam,[35] O. A. Hannuksela,[222] H. Hansen,[2] J. Hanson,[68] R. Harada,[45] A. R. Hardison,[184] S. Harikumar,[99] K. Haris,[223] I. Harley-Trochimczyk,[139] T. Harmark,[147] J. Harms,[47,48] G. M. Harry,[224] I. W. Harry,[76] J. Hart,[109] M. T. Hartman,[21] B. Haskell,[99,225,226] C.-J. Haster,[216] K. Haughian,[90] H. Hayakawa,[54] K. Hayama,[227] A. Heffernan,[136] D. Hegde,[16] M. C. Heintze,[68] J. Heinze,[124] J. Heinzel,[37] H. Heitmann,[118] F. Hellman,[91] A. F. Helmling-Cornell,[81] G. Hemming,[67] O. Henderson-Sapir,[121] M. Hendry,[90] I. S. Heng,[90] M. H. Hennig,[90] C. Henshaw,[62] M. Heurs,[9,10] A. L. Hewitt,[228,229] J. Heynen,[16] J. Heyns,[37] S. Higginbotham,[35] S. Hild,[38,39] S. Hill,[90] Y. Himemoto,[230] N. Hirata,[26] C. Hirose,[231] D. Hofman,[178] B. E. Hogan,[50] N. A. Holland,[39,112] K. Holley-Bockelmann,[150] I. J. Hollows,[177] D. E. Holz,[137] L. Honet,[115] K. M. Hoops,[210] M. E. Hoque,[232] D. J. Horton-Bailey,[91] J. Hough,[90] S. Hourihane,[12] N. T. Howard,[150] E. J. Howell,[6] C. G. Hoy,[76] C. A. Hrishikesh,[22] P. Hsi,[37] H.-F. Hsieh,[154] H.-Y. Hsieh,[154] C. Hsiung,[233] S.-H. Hsu,[234] W.-F. Hsu,[100] Q. Hu,[90] H. Y. Huang,[148] Y. Huang,[8] Y. T. Huang,[82] A. D. Huddart,[235] B. Hughey,[50] V. Hui,[33] S. Husa,[136] L. Iampieri,[41,40] G. A. Iandolo,[38] M. Ianni,[23,22] G. Iannone,[140] J. Iascau,[81] K. Ide,[236] R. Iden,[220] A. Ierardi,[47,48] S. Ikeda,[153] H. Imafuku,[45] Y. Inoue,[148] G. Iorio,[95] P. Iosif,[188,52] J. Irwin,[90] R. Ishikawa,[236] T. Ishikawa,[237] M. Isi,[196] K. S. Isleif,[238] Y. Itoh,[208,239] S. Iwaguchi,[237] M. Iwaya,[207] B. R. Iyer,[25] C. D. Jackson,[49] C. Jacquet,[104] P.-E. Jacquet,[129] T. Jacquot,[43] S. J. Jadhav,[240] S. P. Jadhav,[146] M. Jain,[141] T. Jain,[228] A. L. James,[12] K. Jani,[150] J. Janquart,[16] N. N. Janthalur,[240] S. Jaraba,[241] P. Jaranowski,[242] R. Jaume,[136] W. Javed,[35] M. Jensen,[2] W. Jia,[37] J. Jiang,[103] H.-B. Jin,[243,244] G. R. Johns,[120] N. A. Johnson,[49] R. Johnston,[90] N. Johny,[9,10] D. H. Jones,[36] D. I. Jones,[214] R. Jones,[90] H. E. Jose,[81] P. Joshi,[62] S. K. Joshi,[83] G. Joubert,[61] J. Ju,[245] L. Ju,[6] I. L. Juarez-Reyes,[81] K. Jung,[246] J. Junker,[36] V. Juste,[115] H. B. Kabagoz,[37] T. Kajita,[207] I. Kaku,[208] V. Kalogera,[117] M. Kalomenopoulos,[216] M. Kamiizumi,[54] N. Kanda,[239,208] S. Kandhasamy,[83] G. Kang,[247] J. B. Kanner,[12] S. A. KantiMahanty,[19] S. J. Kapadia,[83] D. P. Kapasi,[59] M. Karthikeyan,[141] M. Kasprzack,[12] H. Kato,[158] T. Kato,[207] E. Katsavounidis,[37] W. Katzman,[68] R. Kaushik,[107] K. Kawabe,[2] R. Kawamoto,[208] D. Keitel,[136] S. A. Kemper,[57] L. J. Kemperman,[121] J. Kennington,[8] F. A. Kerkow,[19] R. Kesharwani,[83] J. S. Key,[248] R. Khadela,[9,10] S. Khadka,[93] S. S. Khadkikar,[8] F. Y. Khalili,[113] F. Khan,[9,10] T. Khanam,[168] M. Khursheed,[107] N. M. Khusid,[195,196] W. Kiendrebeogo,[118,249] N. Kijbunchoo,[121] C. Kim,[250] J. C. Kim,[251] K. Kim,[252] M. H. Kim,[245] S. Kim,[253] Y.-M. Kim,[252] C. Kimball,[117] K. Kimes,[59] M. Kinnear,[35] J. S. Kissel,[2] S. Klimenko,[49] A. M. Knee,[119] E. J. Knox,[81] N. Knust,[9,10] K. Kobayashi,[207] S. M. Koehlenbeck,[93] G. Koekoek,[39,38] K. Kohri,[254] K. Kokeyama,[35,237] S. Koley,[47,170] P. Kolitsidou,[124] A. E. Koloniari,[255] K. Komori,[44,45] K. Kompanets,[19] A. K. H. Kong,[154] A. Kontos,[256] K. Kopczuk,[109] L. M. Koponen,[124] M. Korobko,[30] X. Kou,[19] A. Koushik,[24] N. Kouvatsos,[71] M. Kovalam,[6] T. Koyama,[158] D. B. Kozak,[12] E. Kraja,[67] S. L. Kranzhoff,[38,39] V. Kringel,[9,10] N. V. Krishnendu,[124] S. Kroker,[257] A. Królak,[258,190] K. Kruska,[9,10] J. Kubisz,[259] G. Kuehn,[9,10] A. Kulur Ramamohan,[36] Achal Kumar,[49] Anil Kumar,[240] Praveen Kumar,[181] Prayush Kumar,[25] Rahul Kumar,[2] Rakesh Kumar,[97] Sumit Kumar,[75,39] J. Kume,[260,261,45] K. Kuns,[37] N. Kuntimaddi,[35] S. Kuroyanagi,[262,263] S. Kuwahara,[45] K. Kwak,[246] K. Kwan,[36] S. Kwon,[45] G. Lacaille,[90] D. Laghi,[193] A. H. Laity,[128] A. Lakhal,[129] E. Lalande,[264] M. Lalleman,[24] S. Lalvani,[117] M. Landry,[2] R. N. Lang,[37] J. Lange,[155] R. Langgin,[216] B. Lantz,[93] I. La Rosa,[136] A. Lartaux-Vollard,[43] P. D. Lasky,[7] L. Lavezzi,[29] J. Lawrence,[169] M. Laxen,[68] C. Lazarte,[144] A. Lazzarini,[12] C. Lazzaro,[265,162] P. Leaci,[41,40] L. Leali,[19] Y. K. Lecoeuche,[119] H. W. Lee,[266] J. Lee,[82] K. Lee,[245] R.-K. Lee,[154] R. Lee,[37] Sungho Lee,[267] Sunjae Lee,[245] Y. Lee,[148] I. N. Legred,[12] J. Lehmann,[9,10] L. Lehner,[185] M. Le Jean,[178,122] A. Lemaître,[268] M. Lenti,[66,180] M. Leonardi,[78,79,269] M. Lequime,[42] N. Leroy,[43] M. Lesovsky,[12] N. Letendre,[33] M. Lethuillier,[61] S. E. Levin,[46] Y. Levin,[7] S. Lexmond,[112] K. Leyde,[76] K. L. Li,[270] T. G. F. Li,[100] X. Li,[156] Y. Li,[117] Z. Li,[90] Q. Liang,[151] A. Lihos,[120] E. T. Lin,[154] F. Lin,[148] L. C.-C. Lin,[270] Y.-C. Lin,[154] C. Lindsay,[204] S. D. Linker,[210] A. Liu,[222] G. C. Liu,[233] Jian Liu,[6] S. Liu,[151] F. Llamas Villarreal,[169] J. Llobera-Querol,[136] R. K. L. Lo,[147] J.-P. Locquet,[100] S. C. G. Loggins,[271] M. R. Loizou,[141] L. T. London,[71,37] A. Longo,[65,66] D. Lopez,[170] M. Lopez Portilla,[75] M. Lorenzini,[22,23] A. Lorenzo-Medina,[181] V. Loriette,[43] M. Lormand,[68] G. Losurdo,[186,84] E. Lotti,[141] T. P. Lott IV,[62] J. D. Lough,[9,10] H. A. Loughlin,[37] C. O. Lousto,[114] N. K. Y Low,[130] N. Lu,[36] L. Lucchesi,[84] H. Lück,[9,10] O. Lukina,[37] D. Lumaca,[23] A. P. Lundgren,[272,273] L. Lunghini,[67,34,4] A. W. Lussier,[264] X. Ma,[46] D. M. Macleod,[35] I. A. O. MacMillan,[12] A. Macquet,[43] S. S. Madekar,[138] K. Maeda,[158] S. Maenaut,[100] S. S. Magare,[83] R. M. Magee,[12] E. Maggio,[1] R. Maggiore,[39,112] M. Magnozzi,[31,32] P. Mahapatra,[35] M. Mahesh,[30] S. Majhi,[83] E. Majorana,[41,40] C. N. Makarem,[12] E. Makelele,[109] D. Malakar,[110] J. A. Malaquias-Reis,[20] U. Mali,[194] S. Maliakal,[12] A. Malik,[107] L. Mallick,[171,194] A.-K. Malz,[63] N. Man,[118] M. Mancarella,[102] V. Mandic,[19] V. Mangano,[191,162] B. Mannix,[81] G. L. Mansell,[82,37] M. Manske,[11] M. Mantovani,[67] M. Mapelli,[95,96,274] S. Marchetti,[95,96] C. Marinelli,[105] F. Marion,[33] A. S. Markosyan,[93] A. Markowitz,[12] E. Maros,[12] S. Marsat,[104] F. Martelli,[65,66] I. W. Martin,[90] R. M. Martin,[197] B. B. Martinez,[139] D. A. Martinez,[59] M. Martinez,[138,275] V. Martinez,[135] A. Martini,[78,79] J. C. Martins,[20] D. V. Martynov,[124] E. J. Marx,[37] A. Mascioli,[41,4] L. Massaro,[38,39] A. Masserot,[33] M. Masso-Reid,[90] T. Masters,[109] S. Mastrogiovanni,[40] G. Mastropasqua,[77] T. Matcovich,[55] M. Matiushechkina,[9,10] A. Matte-Landry,[264] L. Maurin,[213] N. Mavalvala,[37] N. Maxwell,[2] G. McCarrol,[68] R. McCarthy,[2] D. E. McClelland,[36] S. McCormick,[68] L. McCuller,[12] L. I. McDermott,[126] S. McEachin,[120] C. McElhenny,[120] G. I. McGhee,[90] K. B. M. McGowan,[150] J. McIver,[119] A. McLeod,[6] T. McRae,[36] R. McTeague,[90] D. Meacher,[11] B. N. Meagher,[82] R. Mechum,[114] Q. Meijer,[75] A. Melatos,[130] C. S. Menoni,[174] F. Mera,[2] R. A. Mercer,[11] L. Mereni,[178] K. Merfeld,[168] E. L. Merilh,[68] G. Merino,[101] J. R. Mérou,[136] J. D. Merritt,[81] M. Merzougui,[118] C. Messick,[11] B. Mestichelli,[47] M. Meyer-Conde,[276] F. Meylahn,[9,10] A. Mhaske,[83] A. Miani,[78,79] H. Miao,[277] I. Michaloliakos,[49] C. Michel,[178] Y. Michimura,[12,45] H. Middleton,[124] D. P. Mihaylov,[109] S. J. Miller,[12] M. Millhouse,[62] E. Milotti,[188,52] V. Milotti,[95] Y. Minenkov,[23] E. M. Minihan,[50] Ll. M. Mir,[138] L. Mirasola,[162,265] C.-A. Miritescu,[138] A. Mishra,[25]

C. Mishra,[111] T. Mishra,[49] A. L. Mitchell,[39,112] J. G. Mitchell,[50] O. Mitchem,[81] S. Mitra,[83] V. P. Mitrofanov,[113] K. Mitsuhashi,[26] R. Mittleman,[37] O. Miyakawa,[54] S. Miyoki,[54] G. Mo,[37] L. Mobilia,[65,66] S. R. P. Mohapatra,[12] S. R. Mohite,[8] M. Molina-Ruiz,[91] M. Mondin,[210] M. Montani,[65,66] C. J. Moore,[228] D. Moraru,[2] A. More,[83] S. More,[83] C. Moreno,[278] E. A. Moreno,[37] G. Moreno,[2] A. Moreso Serra,[86] C. Morgan,[35] S. Morisaki,[207] Y. Moriwaki,[158] G. Morras,[211] A. Moscatello,[95] M. Mould,[37] B. Mours,[69] C. M. Mow-Lowry,[39,112] L. Muccillo,[180,66] F. Muciaccia,[41,40] Arunava Mukherjee,[232] D. Mukherjee,[124] Samanwaya Mukherjee,[25] Soma Mukherjee,[169] Subroto Mukherjee,[97] Suvodip Mukherjee,[14] N. Mukund,[37] A. Mullavey,[68] C. L. Mungioli,[6] M. Murakoshi,[236] P. G. Murray,[90] D. Nabari,[78,79] S. L. Nadji,[9,10] S. Nadji,[178] A. Nagar,[29,279] N. Nagarajan,[90] K. Nakagaki,[54] K. Nakamura,[26] H. Nakano,[280] M. Nakano,[12] D. Nanadoumgar-Lacroze,[138] D. Nandi,[13] V. Napolano,[67] S. U. Naqvi,[111] P. Narayan,[219] I. Nardecchia,[23] T. Narikawa,[207] H. Narola,[75] L. Naticchioni,[281,40] R. K. Nayak,[282] J. Neeson,[35] L. Negri,[75] A. Nela,[90] C. Nelle,[81] A. Nelson,[139] T. J. N. Nelson,[68] A. Nemmani,[99] M. Nery,[9,10] A. Neunzert,[2] M. Newell,[17] S. Ng,[59] L. Nguyen Quynh,[283] A. B. Nielsen,[284] Y. Nishino,[26,285] A. Nishizawa,[286] S. Nissanke,[287,39] W. Niu,[8] F. Nocera,[67] J. Noller,[288] M. Norman,[35] C. North,[35] J. Novak,[241,289] R. Nowicki,[150] J. F. Nuño Siles,[211] G. Nurbek,[169] L. K. Nuttall,[76] K. Obayashi,[236] J. Oberling,[2] C. E. Ochoa,[46] J. O'Dell,[235] M. Oertel,[241,289] G. Oganesyan,[47,48] T. O'Hanlon,[68] M. Ohashi,[54,276] F. Ohme,[9,10] I. Oke,[60] R. Omer,[19] B. O'Neal,[120] M. Onishi,[158] K. Oohara,[290,291] B. O'Reilly,[68] M. Orselli,[55,80] R. O'Shaughnessy,[114] S. Oshino,[54] C. Osthelder,[12] I. Ota,[13] G. Othman,[238] D. J. Ottaway,[121] A. Ouzriat,[61] H. Overmier,[68] B. J. Owen,[108] R. Ozaki,[236] A. E. Pace,[8] R. Pagano,[13] M. A. Page,[26] A. Pai,[199] L. Paiella,[47] A. Pal,[292] S. Pal,[282] M. A. Palaia,[84,85] M. Pálfi,[206] P. P. Palma,[41,22,23] C. Palomba,[40] P. Palud,[21] H. Pan,[154] J. Pan,[6] K.-C. Pan,[154,154] P. K. Panda,[240] Shiksha Pandey,[8] Swadha Pandey,[37] P. T. H. Pang,[39,75] F. Pannarale,[41,40] K. A. Pannone,[59] B. C. Pant,[107] F. H. Panther,[6] M. Panzeri,[65,66] F. Paoletti,[84] A. Paolone,[40,293] A. Papadopoulos,[90] E. E. Papalexakis,[46] L. Papalini,[84,85] G. Papigkiotis,[255] A. Paquis,[43] A. Parisi,[80,55] B.-J. Park,[267] J. Park,[294] W. Parker,[68] G. Pascale,[9,10] D. Pascucci,[98] A. Pasqualetti,[67] R. Passaquieti,[85,84] L. Passenger,[7] D. Passuello,[84] O. Patane,[2] A. V. Patel,[148] D. Pathak,[83] A. Patra,[35] B. Patricelli,[85,84] B. G. Patterson,[35] K. Paul,[111] S. Paul,[81] E. Payne,[12] T. Pearce,[35] M. Pedraza,[12] A. Pele,[12] F. E. Peña Arellano,[295] X. Peng,[124] Y. Peng,[62] S. Penn,[296,82] M. D. Penuliar,[59] A. Perego,[78,79] Z. Pereira,[141] C. Périgois,[297,96,95] G. Perna,[95] A. Perreca,[47,48] J. Perret,[21] S. Perrès,[61] J. W. Perry,[39,112] S. Peters,[170] S. Petracca,[209] C. Petrillo,[80] H. P. Pfeiffer,[1] H. Pham,[68] K. A. Pham,[19] K. S. Phukon,[124] H. Phurailatpam,[222] M. Piarulli,[104] L. Piccari,[41,40] O. J. Piccinni,[36] M. Pichot,[118] A. Pied,[90] M. Piendibene,[85,84] F. Piergiovanni,[65,66] L. Pierini,[40] G. Pierra,[40] V. Pierro,[298,140] M. Pietrzak,[99] M. Pillas,[299] L. Pinard,[178] I. M. Pinto,[298,140,300,34] M. Pinto,[67] B. J. Piotrzkowski,[11] M. Pirello,[2] M. D. Pitkin,[228,90] A. Placidi,[55] E. Placidi,[41,40] M. L. Planas,[136] W. Plastino,[215,23] C. Plunkett,[37] R. Poggiani,[85,84] E. Polini,[118] J. Pomper,[84,85] L. Pompili,[1] J. Poon,[222] E. Porcelli,[39] A. S. Porter,[108] E. K. Porter,[21] C. Posnansky,[8] R. Poulton,[67] J. Powell,[146] G. S. Prabhu,[83] M. Pracchia,[170] B. K. Pradhan,[83] T. Pradier,[69] A. K. Prajapati,[97] K. Prasai,[301] R. Prasanna,[240] P. Prasia,[302] G. Pratten,[124] A. Praveen,[194] G. Principe,[188,52] G. A. Prodi,[78,79] P. Prosperi,[84] P. Prosposito,[22,23] A. Puecher,[1] J. Pullin,[13] P. Puppo,[40] M. Pürrer,[128] H. Qi,[17] M. Qiao,[151] J. Qin,[36] G. Quéméner,[176,122] V. Quetschke,[169] P. J. Quinonez,[50] R. Rading,[238] I. Rainho,[144] S. Raja,[107] C. Rajan,[107] B. Rajbhandari,[114] K. E. Ramirez,[68] F. A. Ramis Vidal,[136] M. Ramos Arevalo,[169] A. Ramos-Buades,[136,39] S. Ranjan,[62] M. Ranjbar,[46] K. Ransom,[68] P. Rapagnani,[41,40] B. Ratto,[50] A. Ravichandran,[141] A. Ray,[117] V. Raymond,[35] M. Razzano,[85,84] J. Read,[59] J. Regan,[216] T. Regimbau,[33] T. Reichardt,[146] S. Reid,[60] C. Reissel,[37] D. H. Reitze,[12] A. I. Renzini,[12,133,134] B. Revenu,[303,43] A. Revilla Peña,[86] L. Ricca,[16] F. Ricci,[41,40] M. Ricci,[40,41] A. Ricciardone,[85,84] J. Rice,[82] J. W. Richardson,[46] M. L. Richardson,[121] A. Rijal,[50] K. Riles,[94] H. K. Riley,[35] S. Rinaldi,[274] J. Rittmeyer,[30] C. Robertson,[235] F. Robinet,[43] M. Robinson,[2] A. Rocchi,[23] L. Rolland,[33] J. G. Rollins,[12] A. E. Romano,[304] R. Romano,[3,4] A. Romero-Rodríguez,[33] I. M. Romero-Shaw,[228] J. H. Romie,[68] S. Ronchini,[8] T. J. Roocke,[121] L. Rosa,[4,34] T. J. Rosauer,[46] C. A. Rose,[62] D. Rosińska,[131] M. P. Ross,[57] M. Rossello-Sastre,[136] S. Rowan,[90] K. Rowlands,[184] S. K. Roy,[195,196] S. Roy,[16] D. Rozza,[133,134] P. Ruggi,[67] N. Ruhama,[246] G. H. Ruiz,[271] E. Ruiz Morales,[305,211] K. Ruiz-Rocha,[150] V. Russ,[179] S. Sachdev,[62] T. Sadecki,[2] P. Saffarieh,[39,112] S. Safi-Harb,[171] M. R. Sah,[14] S. Saha,[154] T. Sainrat,[69] S. Sajith Menon,[218,41,40] K. Sakai,[306] Y. Sakai,[276] M. Sakellariadou,[71] S. Sakon,[8] O. S. Salafia,[164,134,133] F. Salces-Carcoba,[12] L. Salconi,[67] M. Saleem,[155] F. Salemi,[41,40] M. Sallé,[39] S. U. Salunkhe,[83] S. Salvador,[176,175] A. Salvarese,[155] A. Samajdar,[75,39] A. Sanchez,[2] E. J. Sanchez,[12] N. Sanchis-Gual,[144] J. R. Sanders,[184] E. M. Sänger,[1] F. Santoliquido,[47,48] F. Sarandrea,[29] T. R. Saravanan,[83] N. Sarin,[7] P. Sarkar,[9,10] A. Sasli,[19,255] P. Sassi,[55,80] B. Sassolas,[178] B. S. Sathyaprakash,[8,35] R. Sato,[231] S. Sato,[158] Yukino Sato,[158] Yu Sato,[158] O. Sauter,[49] R. L. Savage,[2] T. Sawada,[54] H. L. Sawant,[83] S. Sayah,[178] V. Scacco,[22,23] D. Schaetzl,[12] M. Scheel,[156] A. Schiebelbein,[194] M. G. Schiworski,[82] P. Schmidt,[124] S. Schmidt,[75] R. Schnabel,[30] M. Schneewind,[9,10] R. M. S. Schofield,[81,2] K. Schouteden,[100] B. W. Schulte,[9,10] M. Schulz,[47,48] B. F. Schutz,[35,9,10] E. Schwartz,[307] M. Scialpi,[308] J. Scott,[90] S. M. Scott,[36] R. M. Sedas,[68] T. C. Seetharamu,[90] M. Seglar-Arroyo,[138] Y. Sekiguchi,[309] D. Sellers,[68] N. Sembo,[208] A. S. Sengupta,[310] E. G. Seo,[90] J. W. Seo,[100] V. Sequino,[34,4] M. Serra,[40] A. Sevrin,[192] T. Shaffer,[2] U. S. Shah,[62] M. A. Shaikh,[311] L. Shao,[312] J. Sharkey,[90] A. K. Sharma,[136] Preeti Sharma,[13] Priyanka Sharma,[107] Ritwik Sharma,[19] Sushant Sharma-Chaudhary,[19] P. Shawhan,[132] N. S. Shcheblanov,[313,268] E. Sheridan,[150] Z.-H. Shi,[154] R. Shimomura,[314] H. Shinkai,[314] S. Shirke,[83] D. H. Shoemaker,[37] D. M. Shoemaker,[155] R. W. Short,[2] S. ShyamSundar,[107] A. Sider,[163] H. Siegel,[195,196] V. Sierra,[278] D. Sigg,[2] L. Silenzi,[38,39] L. Silvestri,[41,173] M. Simmonds,[121] L. P. Singer,[315] Amitesh Singh,[219] Anika Singh,[12] D. Singh,[91] M. K. Singh,[35] N. Singh,[136] S. Singh,[220,26] A. M. Sintes,[136] V. Sipala,[191,162] V. Skliris,[35] B. J. J. Slagmolen,[36] T. J. Slaven-Blair,[6] J. Smetana,[124] D. A. Smith,[68] J. R. Smith,[59] L. Smith,[188,52] R. J. E. Smith,[7] W. J. Smith,[150] S. Soares de Albuquerque Filho,[65] K. Somiya,[220] I. Song,[154] S. Soni,[37] V. Sordini,[61] F. Sorrentino,[31] H. Sotani,[316] F. Spada,[84] V. Spagnuolo,[39] A. P. Spencer,[90] P. Spinicelli,[67] A. K. Srivastava,[97] F. Stachurski,[90] C. J. Stark,[120] D. A. Steer,[317] N. Steinle,[171] J. Steinlechner,[38,39] S. Steinlechner,[38,39] N. Stergioulas,[255] P. Stevens,[43] M. StPierre,[128] M. D. Strong,[13] A. Strunk,[2] A. L. Stuver,[106,*] M. Suchenek,[99] S. Sudhagar,[99] Y. Sudo,[236] N. Sueltmann,[30] L. Suleiman,[59] K. D. Sullivan,[13] J. Sun,[251,247] L. Sun,[36] S. Sunil,[97] J. Suresh,[118] B. J. Sutton,[71] P. J. Sutton,[35] K. Suzuki,[220] M. Suzuki,[207] A. Svizzeretto,[80] B. L. Swinkels,[39] A. Syx,[122] M. J. Szczepańczyk,[142] P. Szewczyk,[131] M. Tacca,[39] M. Tagliazucchi,[125,77] H. Tagoshi,[207] S. C. Tait,[12] K. Takada,[207] H. Takahashi,[276] R. Takahashi,[26] A. Takamori,[58] S. Takano,[9,10] H. Takeda,[318,319] K. Takeshita,[220] I. Takimoto Schmiegelow,[47,48] M. Takou-Ayaoh,[82] C. Talbot,[137] M. Tamaki,[207] N. Tamanini,[104] D. Tanabe,[148] K. Tanaka,[54] S. J. Tanaka,[236] S. Tanioka,[35] D. B. Tanner,[49] W. Tanner,[9,10] L. Tao,[46] R. D. Tapia,[8] E. N. Tapia San Martín,[39] C. Taranto,[22,23] A. Taruya,[320] J. D. Tasson,[160] J. G. Tau,[114] A. Tejera,[168] R. Tenorio,[136] H. Themann,[210] A. Theodoropoulos,[144] M. P. Thirugnanasambandam,[83] L. M. Thomas,[12] M. Thomas,[68] P. Thomas,[2] J. E. Thompson,[214] S. R. Thondapu,[107] K. A. Thorne,[68] E. Thrane,[7] J. Tissino,[47,48] A. Tiwari,[83] Pawan Tiwari,[47] Praveer Tiwari,[199] S. Tiwari,[193] V. Tiwari,[124] M. R. Todd,[82] E. Tofani,[40] M. Toffano,[95] A. M. Toivonen,[19] K. Toland,[90] A. E. Tolley,[76] T. Tomaru,[26] V. Tommasini,[12] T. Tomura,[54] H. Tong,[7] C. Tong-Yu,[148] A. Torres-Forné,[144,145] C. I. Torrie,[12] I. Tosta e Melo,[321] E. Tournefier,[33] M. Trad Nery,[118] A. Trapananti,[56,55] R. Travaglini,[77] F. Travasso,[56,55] G. Traylor,[68] M. Trevor,[132] M. C. Tringali,[67] A. Tripathee,[94] G. Troian,[188,52] A. Trovato,[188,52] L. Trozzo,[4] R. J. Trudeau,[12] T. Tsang,[35] S. Tsuchida,[322] K. Tsuji,[237] L. Tsukada,[216] K. Turbang,[192,24] M. Turconi,[118] C. Turski,[98] H. Ubach,[86,87] A. S. Ubhi,[124] N. Uchikata,[207] T. Uchiyama,[54]

R. P. Udall,[119] T. Uehara,[323] K. Ueno,[45] V. Undheim,[284] L. E. Uronen,[222] T. Ushiba,[54] M. Vacatello,[84,85] H. Vahlbruch,[9,10] G. Vajente,[12] J. Valencia,[136] M. Valentini,[112,39] E. Vallejo-Pagès,[138] S. A. Vallejo-Peña,[304] S. Vallero,[29] M. van Dael,[39,324] E. Van den Bossche,[192] J. F. J. van den Brand,[38,112,39] C. Van Den Broeck,[75,39] M. van der Kolk,[112] M. van der Sluys,[39,75] A. Van de Walle,[43] J. van Dongen,[39] K. Vandra,[106] M. VanDyke,[126] H. van Haevermaet,[24] J. V. van Heijningen,[39,112] P. Van Hove,[69] J. Vanier,[264] J. Vanosky,[2] N. van Remortel,[24] M. Vardaro,[38,39] A. F. Vargas,[130] V. Varma,[141] A. Vecchio,[124] G. Vedovato,[96] J. Veitch,[90] P. J. Veitch,[121] S. Venikoudis,[16] J. Venneberg,[37] R. C. Venterea,[19] P. Verdier,[61] M. Vereecken,[16] D. Verkindt,[33] B. Verma,[141] Y. Verma,[107] S. M. Vermeulen,[12] F. Vetrano,[65] A. Veutro,[40,41] A. Viceré,[65,66] S. Vidyant,[82] A. D. Viets,[325] A. Vijaykumar,[194] A. Vilkha,[114] N. Villanueva Espinosa,[144] V. Villa-Ortega,[181] E. T. Vincent,[62] J.-Y. Vinet,[118] S. Viret,[61] S. Vitale,[37] A. Vives,[81] L. Vizmeg,[179] H. Vocca,[80,55] D. Voigt,[30] E. R. G. von Reis,[2] J. S. A. von Wrangel,[9,10] W. E. Vossius,[238] L. Vujeva,[147] S. P. Vyatchanin,[113] J. Wack,[12] L. E. Wade,[109] M. Wade,[109] K. J. Wagner,[114] L. Wallace,[12] E. J. Wang,[93] H. Wang,[220] W. H. Wang,[169] Y. F. Wang,[1] Z. Wang,[151] G. Waratkar,[199] R. L. Ward,[36] J. Warner,[2] M. Was,[33] T. Washimi,[26] N. Y. Washington,[12] B. Weaver,[2] S. A. Webster,[90] N. L. Weickhardt,[30] M. Weinert,[9,10] A. J. Weinstein,[12] R. Weiss,[37,†] L. Wen,[6] K. Wette,[36] C. Wheeler,[68] J. T. Whelan,[114] B. F. Whiting,[49] E. G. Wickens,[76] D. Wilken,[9,10] B. M. Williams,[126] D. Williams,[90] M. J. Williams,[76] N. S. Williams,[1] J. L. Willis,[12] B. Willke,[9,10] M. Wils,[100] L. Wilson,[109] C. W. Winborn,[110] J. Winterflood,[6] C. C. Wipf,[12] G. Woan,[90] J. Woehler,[38,39] N. E. Wolfe,[37] H. T. Wong,[148] I. C. F. Wong,[100] K. Wong,[194] T. Wouters,[75,39] J. L. Wright,[2] M. Wright,[90,75] B. Wu,[82] C. Wu,[154] D. S. Wu,[9,10] H. Wu,[154] K. Wu,[126] Q. Wu,[57] Z. Wu,[104] E. Wuchner,[59] D. M. Wysocki,[11] V. A. Xu,[91] Y. Xu,[136] N. Yadav,[29] H. Yamamoto,[12] K. Yamamoto,[158] T. S. Yamamoto,[45] T. Yamamoto,[54] R. Yamazaki,[236] T. Yan,[124] H. Yang,[277] K. Z. Yang,[19] Y. Yang,[159] Z. Yarbrough,[13] J. Yebana,[136] S.-W. Yeh,[154] A. B. Yelikar,[150] X. Yin,[37] J. Yokoyama,[326,45,44] T. Yokozawa,[54] S. Yuan,[6] H. Yuzurihara,[54] M. Zanolin,[50] M. Zeeshan,[114] T. Zelenova,[67] J.-P. Zendri,[96] M. Zeoli,[16] M. Zerrad,[42] M. Zevin,[117] H. Zhang,[151] L. Zhang,[12] N. Zhang,[62] R. Zhang,[103] T. Zhang,[124] C. Zhao,[6] Yue Zhao,[167] Yuhang Zhao,[21] Z.-C. Zhao,[327] Y. Zheng,[110] H. Zhong,[19] H. Zhou,[82] H. O. Zhu,[6] Z.-H. Zhu,[327,328] Z. Zhu,[114] A. B. Zimmerman,[155] L. Zimmermann,[61] M. E. Zucker,[37,12] J. Black,[8] S. Shandera,[8] D. Jeong,[8]

The LIGO Scientific Collaboration, the Virgo Collaboration, and the KAGRA Collaboration

[1]*Max Planck Institute for Gravitational Physics (Albert Einstein Institute), D-14476 Potsdam, Germany*
[2]*LIGO Hanford Observatory, Richland, WA 99352, USA*
[3]*Dipartimento di Farmacia, Università di Salerno, I-84084 Fisciano, Salerno, Italy*
[4]*INFN, Sezione di Napoli, I-80126 Napoli, Italy*
[5]*University of Warwick, Coventry CV4 7AL, United Kingdom*
[6]*OzGrav, University of Western Australia, Crawley, Western Australia 6009, Australia*
[7]*OzGrav, School of Physics & Astronomy, Monash University, Clayton 3800, Victoria, Australia*
[8]*The Pennsylvania State University, University Park, PA 16802, USA*
[9]*Max Planck Institute for Gravitational Physics (Albert Einstein Institute), D-30167 Hannover, Germany*
[10]*Leibniz Universität Hannover, D-30167 Hannover, Germany*
[11]*University of Wisconsin-Milwaukee, Milwaukee, WI 53201, USA*
[12]*LIGO Laboratory, California Institute of Technology, Pasadena, CA 91125, USA*
[13]*Louisiana State University, Baton Rouge, LA 70803, USA*
[14]*Tata Institute of Fundamental Research, Mumbai 400005, India*
[15]*Centre de Physique Théorique, Aix-Marseille Université, Campus de Luminy, 163 Av. de Luminy, 13009 Marseille, France*
[16]*Université catholique de Louvain, B-1348 Louvain-la-Neuve, Belgium*
[17]*Queen Mary University of London, London E1 4NS, United Kingdom*
[18]*University of California, Davis, Davis, CA 95616, USA*
[19]*University of Minnesota, Minneapolis, MN 55455, USA*
[20]*Instituto Nacional de Pesquisas Espaciais, 12227-010 São José dos Campos, São Paulo, Brazil*
[21]*Université Paris Cité, CNRS, Astroparticule et Cosmologie, F-75013 Paris, France*
[22]*Università di Roma Tor Vergata, I-00133 Roma, Italy*
[23]*INFN, Sezione di Roma Tor Vergata, I-00133 Roma, Italy*
[24]*Universiteit Antwerpen, 2000 Antwerpen, Belgium*
[25]*International Centre for Theoretical Sciences, Tata Institute of Fundamental Research, Bengaluru 560089, India*
[26]*Gravitational Wave Science Project, National Astronomical Observatory of Japan, 2-21-1 Osawa, Mitaka City, Tokyo 181-8588, Japan*
[27]*Advanced Technology Center, National Astronomical Observatory of Japan, 2-21-1 Osawa, Mitaka City, Tokyo 181-8588, Japan*
[28]*Theoretisch-Physikalisches Institut, Friedrich-Schiller-Universität Jena, D-07743 Jena, Germany*
[29]*INFN Sezione di Torino, I-10125 Torino, Italy*
[30]*Universität Hamburg, D-22761 Hamburg, Germany*
[31]*INFN, Sezione di Genova, I-16146 Genova, Italy*
[32]*Dipartimento di Fisica, Università degli Studi di Genova, I-16146 Genova, Italy*
[33]*Univ. Savoie Mont Blanc, CNRS, Laboratoire d'Annecy de Physique des Particules - IN2P3, F-74000 Annecy, France*
[34]*Università di Napoli "Federico II", I-80126 Napoli, Italy*
[35]*Cardiff University, Cardiff CF24 3AA, United Kingdom*
[36]*OzGrav, Australian National University, Canberra, Australian Capital Territory 0200, Australia*

[37] *LIGO Laboratory, Massachusetts Institute of Technology, Cambridge, MA 02139, USA*
[38] *Maastricht University, 6200 MD Maastricht, Netherlands*
[39] *Nikhef, 1098 XG Amsterdam, Netherlands*
[40] *INFN, Sezione di Roma, I-00185 Roma, Italy*
[41] *Università di Roma "La Sapienza", I-00185 Roma, Italy*
[42] *Aix Marseille Univ, CNRS, Centrale Med, Institut Fresnel, F-13013 Marseille, France*
[43] *Université Paris-Saclay, CNRS/IN2P3, IJCLab, 91405 Orsay, France*
[44] *Department of Physics, The University of Tokyo, 7-3-1 Hongo, Bunkyo-ku, Tokyo 113-0033, Japan*
[45] *Research Center for the Early Universe (RESCEU), The University of Tokyo, 7-3-1 Hongo, Bunkyo-ku, Tokyo 113-0033, Japan*
[46] *University of California, Riverside, Riverside, CA 92521, USA*
[47] *Gran Sasso Science Institute (GSSI), I-67100 L'Aquila, Italy*
[48] *INFN, Laboratori Nazionali del Gran Sasso, I-67100 Assergi, Italy*
[49] *University of Florida, Gainesville, FL 32611, USA*
[50] *Embry-Riddle Aeronautical University, Prescott, AZ 86301, USA*
[51] *Dipartimento di Scienze Matematiche, Informatiche e Fisiche, Università di Udine, I-33100 Udine, Italy*
[52] *INFN, Sezione di Trieste, I-34127 Trieste, Italy*
[53] *Tecnologico de Monterrey, Escuela de Ingeniería y Ciencias, 64849 Monterrey, Nuevo León, Mexico*
[54] *Institute for Cosmic Ray Research, KAGRA Observatory, The University of Tokyo, 238 Higashi-Mozumi, Kamioka-cho, Hida City, Gifu 506-1205, Japan*
[55] *INFN, Sezione di Perugia, I-06123 Perugia, Italy*
[56] *Università di Camerino, I-62032 Camerino, Italy*
[57] *University of Washington, Seattle, WA 98195, USA*
[58] *Earthquake Research Institute, The University of Tokyo, 1-1-1 Yayoi, Bunkyo-ku, Tokyo 113-0032, Japan*
[59] *California State University Fullerton, Fullerton, CA 92831, USA*
[60] *SUPA, University of Strathclyde, Glasgow G1 1XQ, United Kingdom*
[61] *Université Claude Bernard Lyon 1, CNRS, IP2I Lyon / IN2P3, UMR 5822, F-69622 Villeurbanne, France*
[62] *Georgia Institute of Technology, Atlanta, GA 30332, USA*
[63] *Royal Holloway, University of London, London TW20 0EX, United Kingdom*
[64] *Department of Astronomical Science, The Graduate University for Advanced Studies (SOKENDAI), 2-21-1 Osawa, Mitaka City, Tokyo 181-8588, Japan*
[65] *Università degli Studi di Urbino "Carlo Bo", I-61029 Urbino, Italy*
[66] *INFN, Sezione di Firenze, I-50019 Sesto Fiorentino, Firenze, Italy*
[67] *European Gravitational Observatory (EGO), I-56021 Cascina, Pisa, Italy*
[68] *LIGO Livingston Observatory, Livingston, LA 70754, USA*
[69] *Université de Strasbourg, CNRS, IPHC UMR 7178, F-67000 Strasbourg, France*
[70] *Dipartimento di Fisica "E.R. Caianiello", Università di Salerno, I-84084 Fisciano, Salerno, Italy*
[71] *King's College London, University of London, London WC2R 2LS, United Kingdom*
[72] *Korea Institute of Science and Technology Information, Daejeon 34141, Republic of Korea*
[73] *International College, Osaka University, 1-1 Machikaneyama-cho, Toyonaka City, Osaka 560-0043, Japan*
[74] *Accelerator Laboratory, High Energy Accelerator Research Organization (KEK), 1-1 Oho, Tsukuba City, Ibaraki 305-0801, Japan*
[75] *Institute for Gravitational and Subatomic Physics (GRASP), Utrecht University, 3584 CC Utrecht, Netherlands*
[76] *University of Portsmouth, Portsmouth, PO1 3FX, United Kingdom*
[77] *Istituto Nazionale Di Fisica Nucleare - Sezione di Bologna, viale Carlo Berti Pichat 6/2 - 40127 Bologna, Italy*
[78] *Università di Trento, Dipartimento di Fisica, I-38123 Povo, Trento, Italy*
[79] *INFN, Trento Institute for Fundamental Physics and Applications, I-38123 Povo, Trento, Italy*
[80] *Università di Perugia, I-06123 Perugia, Italy*
[81] *University of Oregon, Eugene, OR 97403, USA*
[82] *Syracuse University, Syracuse, NY 13244, USA*
[83] *Inter-University Centre for Astronomy and Astrophysics, Pune 411007, India*
[84] *INFN, Sezione di Pisa, I-56127 Pisa, Italy*
[85] *Università di Pisa, I-56127 Pisa, Italy*
[86] *Institut de Ciències del Cosmos (ICCUB), Universitat de Barcelona (UB), c. Martí i Franquès, 1, 08028 Barcelona, Spain*
[87] *Departament de Física Quàntica i Astrofísica (FQA), Universitat de Barcelona (UB), c. Martí i Franqués, 1, 08028 Barcelona, Spain*
[88] *Institut d'Estudis Espacials de Catalunya, c. Gran Capità, 2-4, 08034 Barcelona, Spain*
[89] *Dipartimento di Medicina, Chirurgia e Odontoiatria "Scuola Medica Salernitana", Università di Salerno, I-84081 Baronissi, Salerno, Italy*
[90] *IGR, University of Glasgow, Glasgow G12 8QQ, United Kingdom*
[91] *University of California, Berkeley, CA 94720, USA*
[92] *HUN-REN Wigner Research Centre for Physics, H-1121 Budapest, Hungary*
[93] *Stanford University, Stanford, CA 94305, USA*

[94] *University of Michigan, Ann Arbor, MI 48109, USA*
[95] *Università di Padova, Dipartimento di Fisica e Astronomia, I-35131 Padova, Italy*
[96] *INFN, Sezione di Padova, I-35131 Padova, Italy*
[97] *Institute for Plasma Research, Bhat, Gandhinagar 382428, India*
[98] *Universiteit Gent, B-9000 Gent, Belgium*
[99] *Nicolaus Copernicus Astronomical Center, Polish Academy of Sciences, 00-716, Warsaw, Poland*
[100] *Katholieke Universiteit Leuven, Oude Markt 13, 3000 Leuven, Belgium*
[101] *Centro de Investigaciones Energéticas Medioambientales y Tecnológicas, Avda. Complutense 40, 28040, Madrid, Spain*
[102] *Aix-Marseille Université, Université de Toulon, CNRS, CPT, Marseille, France*
[103] *Northeastern University, Boston, MA 02115, USA*
[104] *Laboratoire des 2 Infinis - Toulouse (L2IT-IN2P3), F-31062 Toulouse Cedex 9, France*
[105] *Università di Siena, Dipartimento di Scienze Fisiche, della Terra e dell'Ambiente, I-53100 Siena, Italy*
[106] *Villanova University, Villanova, PA 19085, USA*
[107] *RRCAT, Indore, Madhya Pradesh 452013, India*
[108] *University of Maryland, Baltimore County, Baltimore, MD 21250, USA*
[109] *Kenyon College, Gambier, OH 43022, USA*
[110] *Missouri University of Science and Technology, Rolla, MO 65409, USA*
[111] *Indian Institute of Technology Madras, Chennai 600036, India*
[112] *Department of Physics and Astronomy, Vrije Universiteit Amsterdam, 1081 HV Amsterdam, Netherlands*
[113] *Lomonosov Moscow State University, Moscow 119991, Russia*
[114] *Rochester Institute of Technology, Rochester, NY 14623, USA*
[115] *Université libre de Bruxelles, 1050 Bruxelles, Belgium*
[116] *Bar-Ilan University, Ramat Gan, 5290002, Israel*
[117] *Northwestern University, Evanston, IL 60208, USA*
[118] *Université Côte d'Azur, Observatoire de la Côte d'Azur, CNRS, Artemis, F-06304 Nice, France*
[119] *University of British Columbia, Vancouver, BC V6T 1Z4, Canada*
[120] *Christopher Newport University, Newport News, VA 23606, USA*
[121] *OzGrav, University of Adelaide, Adelaide, South Australia 5005, Australia*
[122] *Centre national de la recherche scientifique, 75016 Paris, France*
[123] *Univ Rennes, CNRS, Institut FOTON - UMR 6082, F-35000 Rennes, France*
[124] *University of Birmingham, Birmingham B15 2TT, United Kingdom*
[125] *DIFA- Alma Mater Studiorum Università di Bologna, Via Zamboni, 33 - 40126 Bologna, Italy*
[126] *Washington State University, Pullman, WA 99164, USA*
[127] *Cornell University, Ithaca, NY 14850, USA*
[128] *University of Rhode Island, Kingston, RI 02881, USA*
[129] *Laboratoire Kastler Brossel, Sorbonne Université, CNRS, ENS-Université PSL, Collège de France, F-75005 Paris, France*
[130] *OzGrav, University of Melbourne, Parkville, Victoria 3010, Australia*
[131] *Astronomical Observatory, University of Warsaw, 00-478 Warsaw, Poland*
[132] *University of Maryland, College Park, MD 20742, USA*
[133] *Università degli Studi di Milano-Bicocca, I-20126 Milano, Italy*
[134] *INFN, Sezione di Milano-Bicocca, I-20126 Milano, Italy*
[135] *Université de Lyon, Université Claude Bernard Lyon 1, CNRS, Institut Lumière Matière, F-69622 Villeurbanne, France*
[136] *IAC3–IEEC, Universitat de les Illes Balears, E-07122 Palma de Mallorca, Spain*
[137] *University of Chicago, Chicago, IL 60637, USA*
[138] *Institut de Física d'Altes Energies (IFAE), The Barcelona Institute of Science and Technology, Campus UAB, E-08193 Bellaterra (Barcelona), Spain*
[139] *University of Arizona, Tucson, AZ 85721, USA*
[140] *INFN, Sezione di Napoli, Gruppo Collegato di Salerno, I-80126 Napoli, Italy*
[141] *University of Massachusetts Dartmouth, North Dartmouth, MA 02747, USA*
[142] *Faculty of Physics, University of Warsaw, Ludwika Pasteura 5, 02-093 Warszawa, Poland*
[143] *Istituto di Astrofisica e Planetologia Spaziali di Roma, 00133 Roma, Italy*
[144] *Departamento de Astronomía y Astrofísica, Universitat de València, E-46100 Burjassot, València, Spain*
[145] *Observatori Astronòmic, Universitat de València, E-46980 Paterna, València, Spain*
[146] *OzGrav, Swinburne University of Technology, Hawthorn VIC 3122, Australia*
[147] *Niels Bohr Institute, University of Copenhagen, 2100 København, Denmark*
[148] *National Central University, Taoyuan City 320317, Taiwan*
[149] *OzGrav, Charles Sturt University, Wagga Wagga, New South Wales 2678, Australia*
[150] *Vanderbilt University, Nashville, TN 37235, USA*

[151] *University of Chinese Academy of Sciences / International Centre for Theoretical Physics Asia-Pacific, Bejing 100190, China*
[152] *Institute of Physics, National Yang Ming Chiao Tung University, 101 Univ. Street, Hsinchu, Taiwan*
[153] *Kamioka Branch, National Astronomical Observatory of Japan, 238 Higashi-Mozumi, Kamioka-cho, Hida City, Gifu 506-1205, Japan*
[154] *National Tsing Hua University, Hsinchu City 30013, Taiwan*
[155] *University of Texas, Austin, TX 78712, USA*
[156] *CaRT, California Institute of Technology, Pasadena, CA 91125, USA*
[157] *Dipartimento di Ingegneria Industriale (DIIN), Università di Salerno, I-84084 Fisciano, Salerno, Italy*
[158] *Faculty of Science, University of Toyama, 3190 Gofuku, Toyama City, Toyama 930-8555, Japan*
[159] *School of Physical Science and Technology, ShanghaiTech University, 393 Middle Huaxia Road, Pudong, Shanghai, 201210, China*
[160] *Carleton College, Northfield, MN 55057, USA*
[161] *University of Szeged, Dóm tér 9, Szeged 6720, Hungary*
[162] *INFN Cagliari, Physics Department, Università degli Studi di Cagliari, Cagliari 09042, Italy*
[163] *Université Libre de Bruxelles, Brussels 1050, Belgium*
[164] *INAF, Osservatorio Astronomico di Brera sede di Merate, I-23807 Merate, Lecco, Italy*
[165] *Departamento de Matemáticas, Universitat de València, E-46100 Burjassot, València, Spain*
[166] *Montana State University, Bozeman, MT 59717, USA*
[167] *The University of Utah, Salt Lake City, UT 84112, USA*
[168] *Johns Hopkins University, Baltimore, MD 21218, USA*
[169] *The University of Texas Rio Grande Valley, Brownsville, TX 78520, USA*
[170] *Université de Liège, B-4000 Liège, Belgium*
[171] *University of Manitoba, Winnipeg, MB R3T 2N2, Canada*
[172] *INAF, Osservatorio di Astrofisica e Scienza dello Spazio, I-40129 Bologna, Italy*
[173] *INFN-CNAF - Bologna, Viale Carlo Berti Pichat, 6/2, 40127 Bologna BO, Italy*
[174] *Colorado State University, Fort Collins, CO 80523, USA*
[175] *Université de Normandie, ENSICAEN, UNICAEN, CNRS/IN2P3, LPC Caen, F-14000 Caen, France*
[176] *Laboratoire de Physique Corpusculaire Caen, 6 boulevard du maréchal Juin, F-14050 Caen, France*
[177] *The University of Sheffield, Sheffield S10 2TN, United Kingdom*
[178] *Université Claude Bernard Lyon 1, CNRS, Laboratoire des Matériaux Avancés (LMA), IP2I Lyon / IN2P3, UMR 5822, F-69622 Villeurbanne, France*
[179] *Western Washington University, Bellingham, WA 98225, USA*
[180] *Università di Firenze, Sesto Fiorentino I-50019, Italy*
[181] *IGFAE, Universidade de Santiago de Compostela, E-15782 Santiago de Compostela, Spain*
[182] *Dipartimento di Scienze Matematiche, Fisiche e Informatiche, Università di Parma, I-43124 Parma, Italy*
[183] *INFN, Sezione di Milano Bicocca, Gruppo Collegato di Parma, I-43124 Parma, Italy*
[184] *Marquette University, Milwaukee, WI 53233, USA*
[185] *Perimeter Institute, Waterloo, ON N2L 2Y5, Canada*
[186] *Scuola Normale Superiore, I-56126 Pisa, Italy*
[187] *Corps des Mines, Mines Paris, Université PSL, 60 Bd Saint-Michel, 75272 Paris, France*
[188] *Dipartimento di Fisica, Università di Trieste, I-34127 Trieste, Italy*
[189] *Université Côte d'Azur, Observatoire de la Côte d'Azur, CNRS, Lagrange, F-06304 Nice, France*
[190] *National Center for Nuclear Research, 05-400 Świerk-Otwock, Poland*
[191] *Università degli Studi di Sassari, I-07100 Sassari, Italy*
[192] *Vrije Universiteit Brussel, 1050 Brussel, Belgium*
[193] *University of Zurich, Winterthurerstrasse 190, 8057 Zurich, Switzerland*
[194] *Canadian Institute for Theoretical Astrophysics, University of Toronto, Toronto, ON M5S 3H8, Canada*
[195] *Stony Brook University, Stony Brook, NY 11794, USA*
[196] *Center for Computational Astrophysics, Flatiron Institute, New York, NY 10010, USA*
[197] *Montclair State University, Montclair, NJ 07043, USA*
[198] *HUN-REN Institute for Nuclear Research, H-4026 Debrecen, Hungary*
[199] *Indian Institute of Technology Bombay, Powai, Mumbai 400 076, India*
[200] *Centro de Física das Universidades do Minho e do Porto, Universidade do Minho, PT-4710-057 Braga, Portugal*
[201] *Aix Marseille Univ, CNRS/IN2P3, CPPM, Marseille, France*
[202] *CNR-SPIN, I-84084 Fisciano, Salerno, Italy*
[203] *Dipartimento di Ingegneria, Università della Basilicata, I-85100 Potenza, Italy*
[204] *SUPA, University of the West of Scotland, Paisley PA1 2BE, United Kingdom*
[205] *Barry University, Miami Shores, FL 33168, USA*
[206] *Eötvös University, Budapest 1117, Hungary*
[207] *Institute for Cosmic Ray Research, KAGRA Observatory, The University of Tokyo, 5-1-5 Kashiwa-no-Ha, Kashiwa City, Chiba 277-8582, Japan*

[208] *Department of Physics, Graduate School of Science, Osaka Metropolitan University, 3-3-138 Sugimoto-cho, Sumiyoshi-ku, Osaka City, Osaka 558-8585, Japan*
[209] *University of Sannio at Benevento, I-82100 Benevento, Italy and INFN, Sezione di Napoli, I-80100 Napoli, Italy*
[210] *California State University, Los Angeles, Los Angeles, CA 90032, USA*
[211] *Instituto de Fisica Teorica UAM-CSIC, Universidad Autonoma de Madrid, 28049 Madrid, Spain*
[212] *Istituto Nazionale di Astrofisica - Osservatorio di Roma, Viale del Parco Mellini 84 - 00136 Roma, Italy*
[213] *Laboratoire d'Acoustique de l'Université du Mans, UMR CNRS 6613, F-72085 Le Mans, France*
[214] *University of Southampton, Southampton SO17 1BJ, United Kingdom*
[215] *Dipartimento di Ingegneria Industriale, Elettronica e Meccanica, Università degli Studi Roma Tre, I-00146 Roma, Italy*
[216] *University of Nevada, Las Vegas, Las Vegas, NV 89154, USA*
[217] *University of Nottingham NG7 2RD, UK*
[218] *Ariel University, Ramat HaGolan St 65, Ari'el, Israel*
[219] *The University of Mississippi, University, MS 38677, USA*
[220] *Graduate School of Science, Institute of Science Tokyo, 2-12-1 Ookayama, Meguro-ku, Tokyo 152-8551, Japan*
[221] *Institute of Physics, Academia Sinica, 128 Sec. 2, Academia Rd., Nankang, Taipei 11529, Taiwan*
[222] *The Chinese University of Hong Kong, Shatin, NT, Hong Kong*
[223] *Nirula Institute of Technology, Kolkata, West Bengal 700109, India*
[224] *American University, Washington, DC 20016, USA*
[225] *Dipartimento di Fisica, Università degli studi di Milano, Via Celoria 16, I-20133, Milano, Italy*
[226] *INFN, sezione di Milano, Via Celoria 16, I-20133, Milano, Italy*
[227] *Department of Applied Physics, Fukuoka University, 8-19-1 Nanakuma, Jonan, Fukuoka City, Fukuoka 814-0180, Japan*
[228] *University of Cambridge, Cambridge CB2 1TN, United Kingdom*
[229] *University of Lancaster, Lancaster LA1 4YW, United Kingdom*
[230] *College of Industrial Technology, Nihon University, 1-2-1 Izumi, Narashino City, Chiba 275-8575, Japan*
[231] *Faculty of Engineering, Niigata University, 8050 Ikarashi-2-no-cho, Nishi-ku, Niigata City, Niigata 950-2181, Japan*
[232] *Saha Institute of Nuclear Physics, Bidhannagar, West Bengal 700064, India*
[233] *Department of Physics, Tamkang University, No. 151, Yingzhuan Rd., Danshui Dist., New Taipei City 25137, Taiwan*
[234] *Department of Electrophysics, National Yang Ming Chiao Tung University, 101 Univ. Street, Hsinchu, Taiwan*
[235] *Rutherford Appleton Laboratory, Didcot OX11 0DE, United Kingdom*
[236] *Department of Physical Sciences, Aoyama Gakuin University, 5-10-1 Fuchinobe, Sagamihara City, Kanagawa 252-5258, Japan*
[237] *Nagoya University, Nagoya, 464-8601, Japan*
[238] *Helmut Schmidt University, D-22043 Hamburg, Germany*
[239] *Nambu Yoichiro Institute of Theoretical and Experimental Physics (NITEP), Osaka Metropolitan University, 3-3-138 Sugimoto-cho, Sumiyoshi-ku, Osaka City, Osaka 558-8585, Japan*
[240] *Directorate of Construction, Services & Estate Management, Mumbai 400094, India*
[241] *Observatoire Astronomique de Strasbourg, Université de Strasbourg, CNRS, 11 rue de l'Université, 67000 Strasbourg, France*
[242] *Faculty of Physics, University of Białystok, 15-245 Białystok, Poland*
[243] *National Astronomical Observatories, Chinese Academy of Sciences, 20A Datun Road, Chaoyang District, Beijing, China*
[244] *School of Astronomy and Space Science, University of Chinese Academy of Sciences, 20A Datun Road, Chaoyang District, Beijing, China*
[245] *Sungkyunkwan University, Seoul 03063, Republic of Korea*
[246] *Department of Physics, Ulsan National Institute of Science and Technology (UNIST), 50 UNIST-gil, Ulju-gun, Ulsan 44919, Republic of Korea*
[247] *Chung-Ang University, Seoul 06974, Republic of Korea*
[248] *University of Washington Bothell, Bothell, WA 98011, USA*
[249] *Laboratoire de Physique et de Chimie de l'Environnement, Université Joseph KI-ZERBO, 9GH2+3V5, Ouagadougou, Burkina Faso*
[250] *Ewha Womans University, Seoul 03760, Republic of Korea*
[251] *National Institute for Mathematical Sciences, Daejeon 34047, Republic of Korea*
[252] *Korea Astronomy and Space Science Institute, Daejeon 34055, Republic of Korea*
[253] *Department of Astronomy and Space Science, Chungnam National University, 9 Daehak-ro, Yuseong-gu, Daejeon 34134, Republic of Korea*
[254] *Division of Science, National Astronomical Observatory of Japan, 2-21-1 Osawa, Mitaka City, Tokyo 181-8588, Japan*
[255] *Department of Physics, Aristotle University of Thessaloniki, 54124 Thessaloniki, Greece*
[256] *Bard College, Annandale-On-Hudson, NY 12504, USA*
[257] *Technical University of Braunschweig, D-38106 Braunschweig, Germany*
[258] *Institute of Mathematics, Polish Academy of Sciences, 00656 Warsaw, Poland*
[259] *Astronomical Observatory, Jagiellonian University, 31-007 Cracow, Poland*
[260] *Department of Physics and Astronomy, University of Padova, Via Marzolo, 8-35151 Padova, Italy*
[261] *Sezione di Padova, Istituto Nazionale di Fisica Nucleare (INFN), Via Marzolo, 8-35131 Padova, Italy*
[262] *Instituto de Fisica Teorica UAM-CSIC, Universidad Autonoma de Madrid, 28049 Madrid, Spain*

[263]*Department of Physics, Nagoya University, ES building, Furocho, Chikusa-ku, Nagoya, Aichi 464-8602, Japan*
[264]*Université de Montréal/Polytechnique, Montreal, Quebec H3T 1J4, Canada*
[265]*Università degli Studi di Cagliari, Via Università 40, 09124 Cagliari, Italy*
[266]*Department of Computer Simulation, Inje University, 197 Inje-ro, Gimhae, Gyeongsangnam-do 50834, Republic of Korea*
[267]*Korea Astronomy and Space Science Institute (KASI), 776 Daedeokdae-ro, Yuseong-gu, Daejeon 34055, Republic of Korea*
[268]*NAVIER, École des Ponts, Univ Gustave Eiffel, CNRS, Marne-la-Vallée, France*
[269]*Gravitational Wave Science Project, National Astronomical Observatory of Japan (NAOJ), Mitaka City, Tokyo 181-8588, Japan*
[270]*Department of Physics, National Cheng Kung University, No.1, University Road, Tainan City 701, Taiwan*
[271]*St. Thomas University, Miami Gardens, FL 33054, USA*
[272]*Institució Catalana de Recerca i Estudis Avançats, E-08010 Barcelona, Spain*
[273]*Institut de Física d'Altes Energies, E-08193 Barcelona, Spain*
[274]*Institut fuer Theoretische Astrophysik, Zentrum fuer Astronomie Heidelberg, Universitaet Heidelberg, Albert Ueberle Str. 2, 69120 Heidelberg, Germany*
[275]*Institucio Catalana de Recerca i Estudis Avançats (ICREA), Passeig de Lluís Companys, 23, 08010 Barcelona, Spain*
[276]*Research Center for Space Science, Advanced Research Laboratories, Tokyo City University, 3-3-1 Ushikubo-Nishi, Tsuzuki-Ku, Yokohama, Kanagawa 224-8551, Japan*
[277]*Tsinghua University, Beijing 100084, China*
[278]*Universidad de Guadalajara, 44430 Guadalajara, Jalisco, Mexico*
[279]*Institut des Hautes Etudes Scientifiques, F-91440 Bures-sur-Yvette, France*
[280]*Faculty of Law, Ryukoku University, 67 Fukakusa Tsukamoto-cho, Fushimi-ku, Kyoto City, Kyoto 612-8577, Japan*
[281]*Istituto Nazionale di Fisica Nucleare (INFN), Universita di Roma "La Sapienza", P.le A. Moro 2, 00185 Roma, Italy*
[282]*Indian Institute of Science Education and Research, Kolkata, Mohanpur, West Bengal 741252, India*
[283]*Phenikaa Institute for Advanced Study (PIAS), Phenikaa University, Yen Nghia, Ha Dong, Hanoi, Vietnam*
[284]*University of Stavanger, 4021 Stavanger, Norway*
[285]*Department of Astronomy, The University of Tokyo, 7-3-1 Hongo, Bunkyo-ku, Tokyo 113-0033, Japan*
[286]*Physics Program, Graduate School of Advanced Science and Engineering, Hiroshima University, 1-3-1 Kagamiyama, Higashihiroshima City, Hiroshima 739-8526, Japan*
[287]*GRAPPA, Anton Pannekoek Institute for Astronomy and Institute for High-Energy Physics, University of Amsterdam, 1098 XH Amsterdam, Netherlands*
[288]*University College London, London WC1E 6BT, United Kingdom*
[289]*Observatoire de Paris, 75014 Paris, France*
[290]*Graduate School of Science and Technology, Niigata University, 8050 Ikarashi-2-no-cho, Nishi-ku, Niigata City, Niigata 950-2181, Japan*
[291]*Niigata Study Center, The Open University of Japan, 754 Ichibancho, Asahimachi-dori, Chuo-ku, Niigata City, Niigata 951-8122, Japan*
[292]*CSIR-Central Glass and Ceramic Research Institute, Kolkata, West Bengal 700032, India*
[293]*Consiglio Nazionale delle Ricerche - Istituto dei Sistemi Complessi, I-00185 Roma, Italy*
[294]*Department of Astronomy, Yonsei University, 50 Yonsei-Ro, Seodaemun-Gu, Seoul 03722, Republic of Korea*
[295]*Department of Physics, University of Guadalajara, Av. Revolucion 1500, Colonia Olimpica C.P. 44430, Guadalajara, Jalisco, Mexico*
[296]*Hobart and William Smith Colleges, Geneva, NY 14456, USA*
[297]*INAF, Osservatorio Astronomico di Padova, I-35122 Padova, Italy*
[298]*Dipartimento di Ingegneria, Università del Sannio, I-82100 Benevento, Italy*
[299]*Institut d'Astrophysique de Paris, Sorbonne Université, CNRS, UMR 7095, 75014 Paris, France*
[300]*Museo Storico della Fisica e Centro Studi e Ricerche "Enrico Fermi", I-00184 Roma, Italy*
[301]*Kennesaw State University, Kennesaw, GA 30144, USA*
[302]*Government Victoria College, Palakkad, Kerala 678001, India*
[303]*Subatech, CNRS/IN2P3 - IMT Atlantique - Nantes Université, 4 rue Alfred Kastler BP 20722 44307 Nantes CÉDEX 03, France*
[304]*Universidad de Antioquia, Medellín, Colombia*
[305]*Departamento de Física - ETSIDI, Universidad Politécnica de Madrid, 28012 Madrid, Spain*
[306]*Department of Electronic Control Engineering, National Institute of Technology, Nagaoka College, 888 Nishikatakai, Nagaoka City, Niigata 940-8532, Japan*
[307]*Trinity College, Hartford, CT 06106, USA*
[308]*Dipartimento di Fisica e Scienze della Terra, Università Degli Studi di Ferrara, Via Saragat, 1, 44121 Ferrara FE, Italy*
[309]*Faculty of Science, Toho University, 2-2-1 Miyama, Funabashi City, Chiba 274-8510, Japan*
[310]*Indian Institute of Technology, Palaj, Gandhinagar, Gujarat 382355, India*
[311]*Seoul National University, Seoul 08826, Republic of Korea*
[312]*Kavli Institute for Astronomy and Astrophysics, Peking University, Yiheyuan Road 5, Haidian District, Beijing 100871, China*
[313]*Laboratoire MSME, Cité Descartes, 5 Boulevard Descartes, Champs-sur-Marne, 77454 Marne-la-Vallée Cedex 2, France*
[314]*Faculty of Information Science and Technology, Osaka Institute of Technology, 1-79-1 Kitayama, Hirakata City, Osaka 573-0196, Japan*
[315]*NASA Goddard Space Flight Center, Greenbelt, MD 20771, USA*
[316]*Faculty of Science and Technology, Kochi University, 2-5-1 Akebono-cho, Kochi-shi, Kochi 780-8520, Japan*
[317]*Laboratoire de Physique de l'École Normale Supérieure, ENS, (CNRS, Université PSL, Sorbonne Université, Université Paris Cité), F-75005 Paris, France*

[318] The Hakubi Center for Advanced Research, Kyoto University, Yoshida-honmachi, Sakyou-ku, Kyoto City, Kyoto 606-8501, Japan
[319] Department of Physics, Kyoto University, Kita-Shirakawa Oiwake-cho, Sakyou-ku, Kyoto City, Kyoto 606-8502, Japan
[320] Yukawa Institute for Theoretical Physics (YITP), Kyoto University, Kita-Shirakawa Oiwake-cho, Sakyou-ku, Kyoto City, Kyoto 606-8502, Japan
[321] University of Catania, Department of Physics and Astronomy, Via S. Sofia, 64, 95123 Catania CT, Italy
[322] National Institute of Technology, Fukui College, Geshi-cho, Sabae-shi, Fukui 916-8507, Japan
[323] Department of Communications Engineering, National Defense Academy of Japan, 1-10-20 Hashirimizu, Yokosuka City, Kanagawa 239-8686, Japan
[324] Eindhoven University of Technology, 5600 MB Eindhoven, Netherlands
[325] Concordia University Wisconsin, Mequon, WI 53097, USA
[326] Kavli Institute for the Physics and Mathematics of the Universe (Kavli IPMU), WPI, The University of Tokyo, 5-1-5 Kashiwa-no-Ha, Kashiwa City, Chiba 277-8583, Japan
[327] Department of Astronomy, Beijing Normal University, Xinjiekouwai Street 19, Haidian District, Beijing 100875, China
[328] School of Physics and Technology, Wuhan University, Bayi Road 299, Wuchang District, Wuhan, Hubei, 430072, China

(Compiled: April 30, 2026)

ABSTRACT

We report on a gravitational wave search for compact binary coalescences involving at least one component with mass between 0.2 $M_\odot$ to 1 $M_\odot$, and ratio of component masses between 0.1 and 1. The analysis uses data collected by the LIGO detectors between May 24 2023 15:00 UTC and January 16 2024 16:00 UTC. No statistically significant sub-solar mass candidates were identified by the participating search algorithms. We report the detection sensitivity of the current searches to the target sub-solar mass black hole population, while also reporting the sensitivity of the search to low-mass neutron star binaries for the first time. With the absence of detections, we place upper limits on the merger rate of sub-solar mass black holes, ranging from 110 $\mathrm{Gpc}^{-3}\,\mathrm{yr}^{-1}$ to 10000 $\mathrm{Gpc}^{-3}\,\mathrm{yr}^{-1}$ at 90% confidence. We use the merger rate limits to constrain two illustrative dark matter scenarios that can form sub-solar mass compact objects: primordial black holes, and dark black holes forming in a dissipative dark matter model. For late-forming primordial black hole binaries, our search excludes the fraction of dark matter in primordial black holes to be 1 for masses above 0.9 $M_\odot$. In the early-formation scenario, we limit this fraction to be $\leq 7\%$ at 1 $M_\odot$, and $\leq 40\%$ at 0.35 $M_\odot$. For the dissipative model, the excluded region in the parameter space of dark matter fraction in dark black holes and their minimum possible mass extends down to $(1.2\,\text{to}\,1.3)\times10^{-5}$ when the minimum mass is 1 $M_\odot$. For binary neutron stars that include sub-solar mass components, we estimate the sensitive space-time hypervolume to be $\sim10^{-3}$ Gpc^3 yr, and report the upper limit on their merger rate for a simple, fixed population as $\sim$86 $\mathrm{Gpc}^{-3}\,\mathrm{yr}^{-1}$.

1. INTRODUCTION

The LIGO–Virgo–KAGRA Collaboration (LVK; Abbott et al. 2016a) has published over 200 probable gravitational wave (GW) candidates from searches for compact binary coalescences (CBCs) in data from the first observing run (O1; Abbott et al. 2019a), second observing run (O2; Abbott et al. 2021, 2024), third observing run (O3; Abbott et al. 2023a), and the first part of the fourth observing run (O4a; Abac et al. 2025a,b) of the Laser Interferometer Gravitational-Wave Observatory (LIGO; Capote et al. 2025; Ganapathy et al. 2023; Jia et al. 2024; Soni et al. 2025; Martynov et al. 2016; Harry & the LIGO Scientific Collaboration 2010; Abbott et al. 2016b) and Virgo (Acernese et al. 2014) detectors in the latest Gravitational-Wave Transient Catalog, GWTC-4.0 (Abac et al. 2025a,c,d). These candidates are produced by searches targeting binary black holes (BBHs), binary neutron stars (BNSs) and neutron star–black hole binaries (NSBHs) with component masses $\geq 1\,M_\odot$, where the lower bound is motivated observationally by known pulsars, and theoretically by the expectation that neutron star masses should lie near the Chandrasekhar limit for white dwarfs of 1.4 $M_\odot$ dictated by the proton mass and neutron mass (Chandrasekhar 1931). Additionally, black holes produced by stars are expected to have masses exceeding neutron star masses.

Although GW detectors are primarily sensitive to mergers of stellar-mass compact objects, they can also detect signals from less massive binaries of compact objects, if such systems exist in nature (Magee et al. 2018). Targeted searches for sub-solar mass (SSM) compact objects open a window into exotic formation channels that may involve new physics beyond the standard astrophysical paradigm (Singh 2024). A key motivation for these searches is the possibility that some compact objects could be primordial black holes (PBHs) which are a candidate for dark matter (Hawking 1971; Chapline 1975; Green & Kavanagh 2021). PBHs have been proposed to contribute to the population of GW

* Deceased, September 2024.
† Deceased, August 2025.

sources since the first detection of GW150914 (Abbott et al. 2016c; Bird et al. 2016; Sasaki et al. 2016; Clesse & García-Bellido 2017). They are purported to form in the early universe and dominate the merger rate across all redshifts with a peak around $z \geq 30$, compared to the merger rate of stellar black holes, which, if it follows the star formation rate, would peak around $z \sim 1$–2 (Ng et al. 2022, 2023). Even though PBHs can populate a wide mass spectrum extending above a solar mass, we rely on the detection of a sub-solar mass candidate to conclusively distinguish them from stellar black holes (Carr et al. 2021).

GW observations of BBHs can also constrain theories of dissipative dark matter and its chemistry where dark halos gravitationally collapse to form dark black holes (DBHs) in regions of sufficiently high dark matter density (Shandera et al. 2018; Abbott et al. 2023b; Singh et al. 2021). The merger rate of DBHs in this scenario is inversely proportional to the average DBH mass. Therefore, SSM black holes forming from dissipative halos could have a higher predicted merger rate than black holes forming through regular stellar evolutionary channels, which implies that SSM searches can provide strict limits on dissipative dark matter models (Shandera et al. 2018). Especially if the lowest possible DBH mass is smaller than the white dwarf Chandrasekhar limit, we can start to probe the particle nature of dissipative dark matter using SSM searches.

Additionally, models where accumulation of non-annihilating dark matter transmutes neutron stars (NSs) to black holes (BHs) with masses below the $2.5\,M_\odot$ maximum NS mass have been constrained using limits on merger rates from O3 SSM searches. Non-detections of these low-mass black holes provide upper limits on the interaction cross-section of dark matter particles with nucleons for GeV scale dark matter (Bhattacharya et al. 2023).

SSM searches have been performed in data from LIGO and Virgo since initial LIGO's science runs (Abbott et al. 2005, 2008, 2018, 2019b, 2022, 2023b; Nitz & Wang 2021a,b; Phukon et al. 2021). LVK SSM searches have probed masses down to $0.2\,M_\odot$; this parameter space initially motivated by the gravitational microlensing surveys of the LMC which suggested that $\sim$ 20% of the Galactic halo is composed of massive compact halo objects with masses in the range $0.15\,M_\odot$ to $0.9\,M_\odot$ (Abbott et al. 2005). Since O2, our SSM searches have allowed for spinning components, initially with dimensionless spin magnitudes $\leq$ 0.1 (Abbott et al. 2019b). In O3, we increased the primary component's mass to $10\,M_\odot$ to include systems with more asymmetric masses, while also increasing the maximum dimensionless spin magnitude to 0.9 for compact objects with component masses greater than $0.5\,M_\odot$ (Abbott et al. 2022, 2023b; Brown et al. 2012), settings we continue to use in O4a. Although PBH and DBH formation scenarios can populate the mass spectrum below $0.2\,M_\odot$, the target parameter space is restricted to alleviate the computational cost of the search. Moreover, the horizon distance of LIGO and Virgo detectors decreases with decreasing mass (Abbott et al. 2018; Allen et al. 2012; Fairhurst & Brady 2008).

The absence of confident detections in previous runs has provided useful constraints on the abundance of PBHs, and dissipative dark matter models (Abbott et al. 2023b). Motivated by the SSM searches' sensitivity to typical electromagnetically-bright sources, for the first time we operate two independent low-latency SSM searches during the fourth observing run (O4) to enable prompt follow-up in the event of a significant candidate (Alléné et al. 2025; Hanna et al. 2025). These real-time searches were followed with archival searches which provide for the determination of the significance of candidates using the noise background collected over the entire observing run. In this paper, we focus on results from the archival SSM searches performed by three pipelines: GstLAL, MBTA and PyCBC. We report their detection sensitivities for SSM BBHs and BNSs by repeating the searches on strain data from O4a with simulated signals added. Further, we derive limits on the merger rate of SSM BBHs, which are used to update the constraints on the fraction of dark matter in PBHs and the fraction of dark matter in DBHs. For the PBH scenario, we present constraints across the component-mass plane in addition to previously used point-mass distributions (Abbott et al. 2018, 2019b, 2022, 2023b).

In addition to our constraints on specific dark matter models, we report the sensitivity of the SSM search to binaries comprising one or two low-mass NSs. SSM searches cover the range of BNS chirp masses, while extending into the high-spin parameter space typically excluded in template-bank based searches for BNS (Abac et al. 2025a). Although matter effects involving the tidal interaction of the binary components influence binary phasing starting at an effective fifth post-Newtonian order, and affect BNS waveforms at ≥ 1 kHz where LIGO and Virgo have reduced sensitivity, the extremely large tides at low NS masses ($\leq 0.5\,M_\odot$) can result in significant mismatches between the BBH template waveforms and the BNS waveform describing the GW signal (Bandopadhyay et al. 2023). Therefore, we extend our sensitivity estimation to include simulated signals from SSM NS mergers (Metzger et al. 2024; Chen & Metzger 2025) to determine the detection efficiency for this population.

2. SEARCH

We report results from three independent search pipelines, described in Sections 2.1, 2.2 and 2.3, which analyzed data collected during O4a, from 24 May 2023 15:00:00 UTC to 16 January 2024 16:00:00 UTC, and the preceding engineer-

ing run, specifically the period of coincident operation of the two LIGO detectors from 15 May 2023 14:13:22 UTC to 19 May 2023 17:31:33 UTC. Details on the detector sensitivity during O4a can be found in Abac et al. (2025c), while detector characterization and data quality in O4a are described in Soni et al. (2025) and Abac et al. (2025d), respectively. All three pipelines employ matched-filtering techniques (Abac et al. 2025d), where the data is correlated with banks of CBC waveform models (hereafter referred to as templates) that span a common parameter space across all pipelines, yielding the signal-to-noise ratio (SNR) for each candidate event. The template banks are designed to search for CBCs with redshifted primary masses $(1+z)m_1$ between $0.2\,M_\odot$ and $10.0\,M_\odot$, and redshifted secondary masses $(1+z)m_2$ between $0.2\,M_\odot$ and $1.0\,M_\odot$. The mass ratio m_2/m_1 ($m_2 \leq m_1$) is restricted within 0.1–1.0 to maintain a computationally manageable number of templates in the bank. We include spin–spin and spin–orbit interaction effects, assuming that the spin vectors of the two bodies are aligned or anti-aligned with the orbital angular momentum vector. The dimensionless spin magnitudes satisfy $\chi_{1,2} \leq 0.9$ for $(1+z)m_{1,2} \geq 0.5\,M_\odot$ and $\chi_{1,2} \leq 0.1$ for $(1+z)m_{1,2} \leq 0.5\,M_\odot$. This search covers the same parameter space as the LVK SSM search performed on O3 data, making a trade-off between possible astrophysical targets and the computational cost of matched-filtering searches in this low-mass region. All pipelines design template banks with a minimal match of ~ 0.97, ensuring that no more than 10% of astrophysical signals are lost due to the discretization of the parameter space (Owen 1996). Although the sensitivity bands of LIGO and Virgo extend down to approximately 15 Hz (Abac et al. 2025c), our templates are truncated to start at higher frequencies, chosen independently by each pipeline, to reduce the computational cost, since GW signals from low-mass CBCs can last for several minutes within the detector band. Details about the SSM template bank generation, search optimization including low-frequency cutoffs, and waveform models specific to each pipeline are provided in the following subsections.

2.1. GstLAL

GstLAL (Cannon et al. 2012; Messick et al. 2017; Sachdev et al. 2019; Hanna et al. 2020; Cannon et al. 2020; Sakon et al. 2024; Tsukada et al. 2023) is a GStreamer-based pipeline that searches for GW signals from CBCs using matched-filtering techniques. A concise overview of the methods developed and adopted for O4 analyses, including the latest archival search workflow employed in this work, is provided in Abac et al. (2025d); Joshi et al. (2025a,b). Unlike in O3 (Abbott et al. 2022, 2023b), GstLAL uses a bin-dependent gating procedure to mitigate glitches instead of the iDQ algorithm (Huxford et al. 2024).

In contrast to previous SSM searches, GstLAL generated the SSM template bank using a geometric placement method manifold (Hanna et al. 2023). This SSM template bank spans the parameter space described above but is constructed with a slightly lower minimum match of 0.965 (Hanna et al. 2025) to limit its size. The resulting bank comprises over 3.0 million templates (Hanna et al. 2025). Templates are modeled using IMRPhenomD (Khan et al. 2016; Husa et al. 2016) with a low-frequency cutoff of at least 45 Hz and a high-frequency cutoff of 1024 Hz. Template waveforms are restricted to a maximum duration of approximately 128 s prior to merger, which may truncate the waveform relative to one starting at 45 Hz. A detailed description of the geometric placement method, as well as the design and performance of the bank, is given in Hanna et al. (2025).

The current SSM search includes several enhancements made in O4 GstLAL analyses relative to the O3 analysis (Abbott et al. 2023a). These include an improved likelihood function (Tsukada et al. 2023), a new singular value decomposition (SVD)-based grouping method for parallelization (Sakon et al. 2024), and a template weighting derived from the manifold mass model (Ray et al. 2023; Abac et al. 2025d). Like the O3 SSM search, we continue to assume a uniform population model due to the lack of observational constraints. The data are match-filtered using the same frequency and waveform duration cutoffs applied in the template bank generation, with waveform models chosen based on redshifted chirp mass $(1+z)\mathcal{M} = (1+z)(m_1 m_2)^{3/5}/(m_1 + m_2)^{1/5}$: the TaylorF2 approximant (Buonanno et al. 2009; Pan et al. 2008; Boyle et al. 2009) is used for $(1+z)\mathcal{M} \leq 1.73\,M_\odot$, and the SEOBNRv4ROM approximant (Buonanno et al. 2009; Bohé et al. 2017; Cotesta et al. 2020) for $(1+z)\mathcal{M} > 1.73\,M_\odot$. After matched-filtering, triggers—potential GW signals in data—are ranked using a likelihood function (Tsukada et al. 2023; Cannon et al. 2015). The likelihood term for multi-detector signal consistency (Hanna et al. 2020) is evaluated over a frequency range of 45 Hz to 512 Hz for this search. Although this high-frequency cutoff is lower than 1024 Hz used in template whitening, we find negligible difference in signal weighting between cutoffs of 512 Hz and 1024 Hz for this likelihood term. Ultimately, all triggers are assigned a false alarm rate (FAR) which quantifies the significance of a candidate signal by comparing it to the distribution of likelihoods for non-astrophysical events.

2.2. MBTA

The Multi-Band Template Analysis (MBTA; Abadie et al. 2012; Adams et al. 2016; Aubin et al. 2021; Alléné et al. 2025) is a matched-filtering-based pipeline that searches for GWs from CBCs in data from the LIGO–Virgo–KAGRA detectors. MBTA stands out by its approach of splitting the matched-filtering process across multiple frequency bands to

optimize computational efficiency (Abac et al. 2025d). This approach significantly reduces the computational cost associated with processing a large template bank.

The template bank used by MBTA is the same as the one employed in the low-latency analysis described in Alléné et al. (2025). It comprises more than 2.5 million templates, covering the parameter space described above, and was generated using a geometric placement algorithm (Brown et al. 2013). The waveforms used to build the template bank are computed using the second-order post-Newtonian TaylorF2 (Buonanno et al. 2009; Pan et al. 2008; Boyle et al. 2009), while the SpinTaylorT4 approximant (Isoyama et al. 2020) is used for the analysis. A low-frequency cutoff of 45 Hz and high-frequency cutoff of 1000 Hz are applied to limit the duration of the templates, ensuring that the filtering remains computationally manageable while preserving the search sensitivity (Alléné et al. 2025).

As an improvement over O3, MBTA now includes a single-detector trigger search in its archival analysis (Alléné et al. 2025), enhancing sensitivity and enabling the use of periods when only one of the two LIGO detectors is operational. The post-processing procedure has also been refined with the implementation of a new internal data quality assessment tool called the SNR-Excess technique which is detailed in Alléné et al. (2025).

2.3. PyCBC

The PyCBC pipeline (Allen et al. 2012; Dal Canton et al. 2014; Usman et al. 2016; Nitz et al. 2017; Davies et al. 2020; Nitz et al. 2024) performs a matched-filtering analysis to detect GW signals from CBCs. The PyCBC SSM search employs the latest version of the pipeline, described in detail in Abac et al. (2025d). However, specific choices were made here to tailor the analysis to the search for SSM compact objects and improve its sensitivity. These changes are summarized below.

The ranking statistic is the same as in the O3 SSM search (Abbott et al. 2022), with the only difference being that corrections for short term variations of the noise power spectral density (PSD) (Mozzon et al. 2020) are not included. The PyCBC SSM template bank contains approximately 2.0 million templates, and was generated using a geometric placement algorithm (Brown et al. 2013). The TaylorF2 post-Newtonian approximant (Buonanno et al. 2009; Pan et al. 2008; Boyle et al. 2009), a low-frequency cutoff of 45 Hz, and a high-frequency cutoff of 1000 Hz were adopted to compute the matches between templates.

The pipeline starts filtering the data at 30 Hz, with a maximum allowed template duration of 1008 s imposed to keep computational resources usage under control. This limit affects only about 6% of the templates, those with the lowest masses, increasing their starting frequency to approximately 33 Hz at most. This choice was found to increase the sensitivity compared to the more straightforward approach of starting from 45 Hz. By contrast, using 30 Hz as the low-frequency cutoff for bank generation would have required a substantially larger number of templates, making the search computationally impractical. The SEOBNRv4ROM approximant (Buonanno et al. 2009; Bohé et al. 2017; Cotesta et al. 2020) is used instead of TaylorF2 for waveform generation when the redshifted total mass $(1+z)(m_1+m_2) > 1.0\,M_\odot$.

Analogously to MBTA, starting in O4, PyCBC includes single-detector triggers in this archival analysis following Davies & Harry (2022). This increases overall sensitivity, and allows for detection of events occurring when only one detector is observing.

2.4. *Results*

We report no significant GW transients from SSM candidates in GstLAL, MBTA and PyCBC search analyses conducted on O4a data. All observed triggers are statistically consistent with a Poisson distribution of noise background events, except for a single outlier corresponding to the published event GW230529_181500 (Abac et al. 2024b). This outlier, identified as the most significant trigger by both GstLAL and PyCBC, is a single-detector event observed at the LIGO Livingston Observatory (LLO). GW230529_181500 is the second-most significant trigger in the MBTA SSM search because it is down-ranked by MBTA's more conservative significance assignment for single-detector events. The secondary mass of this trigger is inferred to exceed one solar mass (Abac et al. 2024b), indicating that it does not contain an SSM candidate. Figure 1 presents the results from GstLAL (left panel), MBTA (middle panel), and PyCBC (right panel), showing the number of events with assigned significance above a given FAR threshold as a function of the threshold.

Table 1 lists triggers from GstLAL, MBTA, and PyCBC with a FAR below 2 yr^{-1}, including those associated with GW230529_181500. The most significant MBTA trigger is consistent with the expected background and shows no coincidence with any significant triggers from other pipelines. The second most significant GstLAL trigger, listed fifth in Table 1, was coincidentally recovered with the same $(1+z)m_1$ and $(1+z)m_2$ as GW230529_181500 at 2023 May 28 11:07:32.09 UTC, but appears to be consistent with the background distribution. MBTA and PyCBC recover this trigger with FARs well above the 2 yr^{-1}, and GWTC-4.0 reports it as GW230528_110748 with even lower significance (Abac et al. 2025a).

Considering that the only significant trigger corresponds to GW230529_181500 (Abac et al. 2024b) and that the second most significant GstLAL trigger is consistent with noise, we

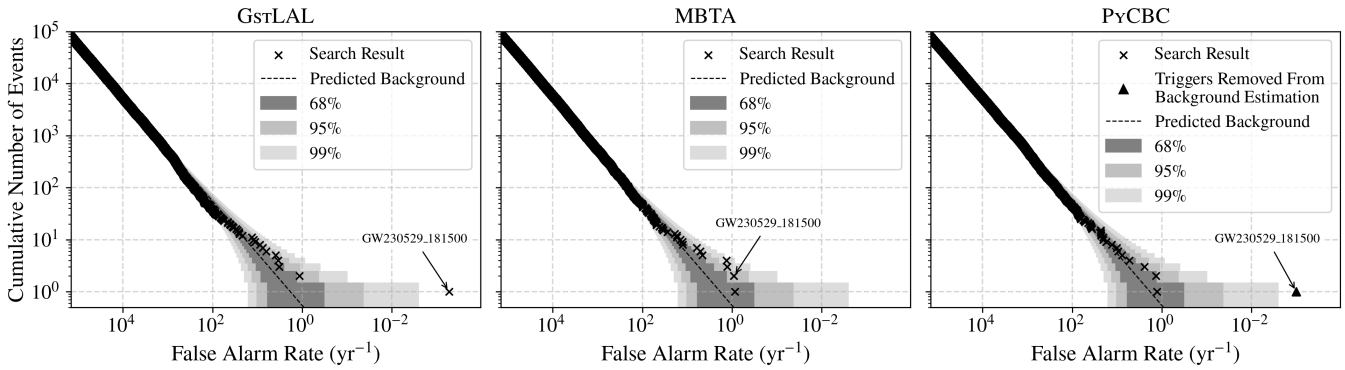

Figure 1. Cumulative number of SSM candidate events as a function of the FAR (in yr^{-1}) for the GstLAL (left panel), MBTA (middle panel), and PyCBC (right panel) analyses. The black dashed curve shows the predicted background with the shaded regions indicating the 68%, 95%, and 99% confidence intervals for the expected background count at each FAR threshold, derived from a Poisson distribution given the total analyzed time of O4a. The observed cumulative count from each pipeline is shown as black crosses at each threshold. The high-significance trigger seen in the GstLAL and PyCBC distributions corresponds to GW230529_181500 from GWTC-4.0 (Abac et al. 2024b), whose inferred secondary mass exceeds one solar mass. Therefore, it is not considered an SSM candidate. In the PyCBC plot, GW230529_181500 is marked with a black triangle indicating that it is not considered in the cumulative count because the analysis removes events with FARs ≤ 1 per 100 yr to reduce contamination from loud signals during background estimation for less significant triggers (Abbott et al. 2016d; Nitz et al. 2019). No other deviation from the expected background is observed, indicating we find no significant GW transient from SSM candidates.

conclude that no significant GW transient from SSM candidates are observed.

3. SEARCH SENSITIVITY

We quantify the sensitivity of our searches with the O4a detector network to GW signals from SSM CBCs to set an upper limit on their merger rates. Due to the changing sensitivity across the observing run and the complex nature of the detection process, we determine this sensitivity empirically via the procedure laid out in Abac et al. (2025d,e); Essick et al. (2025). Following Essick et al. (2025), we simulate and inject signals into detector strain data, and all pipelines perform the search described in Section 2 on this augmented data. Any statement of our sensitivity to SSM sources depends on the assumed astrophysical population that describes their distribution of masses and spins. Therefore, we state the sensitivity to SSM sources *as a function of an assumed population*. This allows us to use the results from a single injection-recovery analysis to determine the sensitivity to multiple population models.

The sensitive space-time hypervolume $\langle VT \rangle$, and its corresponding uncertainty $\sigma_{\langle VT \rangle}$ for an assumed population denoted by $\mathbf{\Lambda}$ is given by

$$\langle VT \rangle(\mathbf{\Lambda}) = \xi(\mathbf{\Lambda}) VT_{\text{total}}, \tag{1}$$

$$\sigma_{\langle VT \rangle} = VT_{\text{total}} \sigma_{\xi}, \tag{2}$$

$$VT_{\text{total}} = T_{\text{obs}} \int_0^{z_{\text{max}}} \mathrm{d}z \frac{1}{1+z} \frac{\mathrm{d}V_c}{\mathrm{d}z}, \tag{3}$$

where $\xi(\mathbf{\Lambda})$ is the fraction of detectable mergers which depends on a chosen detection threshold, VT_{total} is the hypervolume spanned by the injected population assuming a constant number of events per unit time per unit comoving volume within a sphere of redshift z_{max}, σ_{ξ} is the square root of the variance in the estimate of ξ, and T_{obs} denotes the time spanned by the augmented data containing simulated signals, which in this case is the duration of O4a.

We consider two fiducial populations from which simulated sources are drawn to assess the sensitivity of the search: a BBH population with at least one SSM component, and a BNS population, which includes tidal interaction effects, extending into the sub-solar regime. The BBH population is largely similar to previously considered fiducial populations (Abbott et al. 2023b), but an SSM BNS population has not been considered for such studies previously. If SSM BNS systems exist, their GW signals will exhibit effects due to tidal interactions. These effects are significantly more pronounced for low-mass NSs, so the sensitivity of the SSM search will depend on the composition of the assumed population. We model the BNS signals using the IMRPhenomXP_NRTidalv3 waveform model (Pratten et al. 2021; Abac et al. 2024a) with tidal effects given by the GPPVA+DD2 equation of state (Servignat et al. 2024) as implemented in the LALSuite library for GW data analysis (LIGO–Virgo–KAGRA Collaboration 2018). Tidal effects for systems including low-mass NSs are extrapolated from those found in numerical simulations of systems with components above $1\,M_{\odot}$. However, this equation of state produces large-radius stars with tides near the upper limit allowed by previous GW observations (Abbott et al. 2017; Radice et al. 2018), so should give a reasonably conservative estimate for our sensitivity to SSM BNSs using template waveforms that do not include tides.

Table 1. Triggers recovered with a FAR below 2 yr^{-1} by GstLAL, MBTA and PyCBC.

FAR (yr^{-1})	Pipeline	UTC	$(1+z)m_1$ ($M_\odot$)	$(1+z)m_2$ ($M_\odot$)	χ_1	χ_2	Inst.	Network SNR
0.00052	GstLAL	2023 May 29 18:15:00.75 UTC	6.49	0.98	0.27	0.27	L	10.63
0.0010	PyCBC	2023 May 29 18:15:00.75 UTC	7.73	0.87	0.43	−0.64	L	11.10
0.87	MBTA	2023 September 14 21:02:19.50 UTC	2.63	0.29	−0.72	−0.02	HL	9.44
0.91	MBTA	2023 May 29 18:15:00.75 UTC	7.64	0.88	0.39	−0.07	L	9.96
1.2	GstLAL	2023 May 28 11:07:32.09 UTC	6.49	0.98	0.73	0.73	HL	9.48
1.3	PyCBC	2023 July 19 11:50:50.27 UTC	0.74	0.24	−0.24	0.10	HL	9.47
1.3	MBTA	2023 October 14 08:15:06.33 UTC	2.28	0.22	0.90	0.05	HL	10.28
1.3	MBTA	2023 August 10 07:13:47.88 UTC	1.86	0.32	0.65	−0.10	L	12.16
1.4	PyCBC	2023 August 10 10:10:03.37 UTC	0.60	0.21	0.87	−0.07	HL	9.43

Note—We report the redshifted masses $(1+z)m_{1,2}$ and the dimensionless spin magnitudes $\chi_{1,2}$ of the primary (1) and secondary (2) components corresponding to the template that yielded the highest ranking statistic for each trigger. The Network SNR is defined as the square root of the quadrature sum of the SNR measured in all detectors operating at the time of the trigger. The detectors which were observing at the time of each event are listed under the 'Inst.' column, denoted by H for LIGO Hanford and L for LIGO Livingston. Triggers corresponding to GW230529_181500 (Abac et al. 2024b) in results from GstLAL, PyCBC, and MBTA appear as the first, second, and fourth entries respectively.

Table 2 summarizes the properties of the BBH and BNS fiducial populations ($\mathbf{\Lambda}_0$). The lowest component mass for the BBH population is chosen in accordance with the search parameter space which extends to $0.2\,M_\odot$. For BNSs, we restrict component masses to be greater than $0.5\,M_\odot$. At $0.5\,M_\odot$, tidal effects extrapolated for the GPPVA+DD2 equation of state are on the order of 10^5 and would be even higher at lower NS masses, thereby exacerbating systematic uncertainties from waveform validity. The secondary component mass is restricted such that every source has at least one sub-solar mass component. For both populations, we choose an equally weighted mixture model of a half normal distribution and a Beta distribution such that the dimensionless spin magnitude peaks at $\chi_{1,2} = 0$ with small support extending to high spins. This choice is motivated by expected low spins for primordial black holes (García-Bellido 2017; Chiba & Yokoyama 2017; De Luca et al. 2019, 2020), and observed low spins for Galactic BNS (Stovall et al. 2018) without excluding support for highly-spinning systems entirely. The component spins are isotropically distributed, i.e. the cosine of the angles between the orbital angular momentum vector and the component spin vectors are distributed uniformly. The sources are distributed uniformly in comoving volume up to a maximum redshift $z_{\mathrm{max}} = 0.2$ which results in a total hypervolume $VT_{\mathrm{total}} = 1.65\,\mathrm{Gpc}^3\,\mathrm{yr}$.

Details on the calculation of the fraction of detectable mergers, $\xi(\mathbf{\Lambda})$ using searches performed on the fiducial injection population ($\mathbf{\Lambda}_0$) are provided in Appendix A. The choice of FAR thresholds for estimating $\xi(\mathbf{\Lambda})$ are described in relevant sections. We use the software package GWPopulation (Talbot et al. 2025) to compute the fraction of detectable mergers $\xi(\mathbf{\Lambda})$ through importance sampling (Equation A2), and finally compute the sensitive hypervolume $\langle VT \rangle$ (Equation 1). The following subsections detail the $\langle VT \rangle$ for selected BBH and BNS models. Additionally, we provide the complete injection datasets and search results in a supplemental data release (LIGO–Virgo–KAGRA Collaboration 2026), allowing for the reweighting of these fiducial results to alternative populations.

3.1. *Sub-solar mass BBH*

We report the $\langle VT \rangle$ for BBH systems with at least one component less massive than $1\,M_\odot$ as a function of the chirp mass $\mathcal{M}$ of the binary. The fiducial population ($\mathbf{\Lambda}_0$; Table 2) which is log-uniform in component masses, is re-weighted in its spin distribution to be isotropic and with uniform component spin magnitudes $\chi_{1,2} \leq 0.1$; in addition, the mass ratio is restricted to the range $m_2/m_1 \geq 0.05$ to match the BBH distribution considered in Abbott et al. (2023b) and ensure that $\langle VT \rangle$ from O4a is directly comparable with $\langle VT \rangle$ from O3.

We use the FAR of the most significant noise candidate from O4a data as the detection threshold to calculate $\langle VT \rangle$, allowing for the calculation of upper limits on the merger rate through the loudest event statistic formalism (Biswas et al. 2009). Specifically, we assume FAR thresholds of $1.2\,\mathrm{yr}^{-1}$, $0.87\,\mathrm{yr}^{-1}$ and $1.3\,\mathrm{yr}^{-1}$ for GstLAL, MBTA and PyCBC respectively.

The total $\langle VT \rangle$ of our search is dominated by the more massive systems in the population model. In order to provide a more refined estimate of our sensitivity across mass space, and in order to compare to previously reported results from O3 (Abbott et al. 2023b), we estimate our sensitivity in individual mass bins. Such bin-wise estimates also par-

tially mitigate, but do not remove entirely, the systematic uncertainty in our $\langle VT \rangle$ estimate due to having to choose a population model. Figure 2 shows the $\langle VT \rangle$ computed over O4a as a function of $\mathcal{M}$ for the three searches separately, with $\langle VT_{\rm O3} \rangle$ plotted for comparison. We divide the range of chirp masses into 8 linearly spaced bins between 0.16 $M_\odot$ to 2.44 $M_\odot$. The simulated signals which pass the detection threshold are reweighted to the desired population ($\mathbf{\Lambda}$) described above using Equation (A2) to compute the $\langle VT \rangle$ within each $\mathcal{M}$ bin. The $\langle VT \rangle_{\rm O4a}$ for the three searches remains similar to the $\langle VT \rangle_{\rm O3}$, as the expected gain from improved sensitivity of the detectors and searches in O4 is offset by the shorter observing period of 0.76 yr in O4a compared to 0.9 yr in O3. The mean ratio of $\langle VT \rangle_{\rm O4a}$ to $\langle VT \rangle_{\rm O3}$ across all $\mathcal{M}$ bins is 1.1, 1.0, and 1.3 for GstLAL, MBTA, and PyCBC respectively. The appreciable increase for PyCBC is partly due to to the reduced low-frequency cutoff of 30 Hz in the O4a analysis.

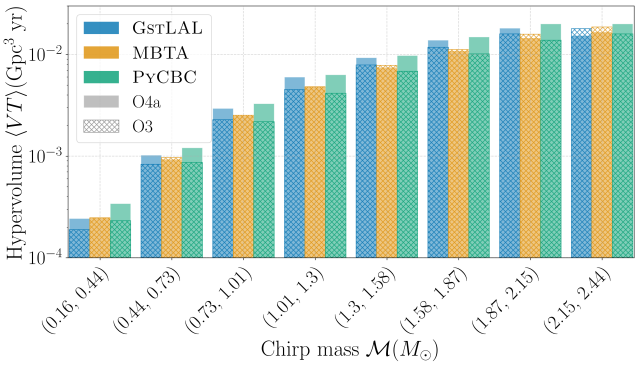

Figure 2. Sensitive hypervolume, $\langle VT \rangle$ (Gpc^3 yr) as a function of the chirp mass, $\mathcal{M}$ for searches GstLAL (*blue*), MBTA (*yellow*) and PyCBC (*green*). The masses of the detected sources within each $\mathcal{M}$ bin are reweighted to a log-uniform distribution with 0.19 $M_\odot \leq m_2 \leq 1.1\,M_\odot$ and $m_2 \leq m_1 \leq 11.1\,M_\odot$ with $q \geq 0.05$, and their spin distribution is reweighted to an isotropic uniform distribution with $\chi_{1,2} \leq 0.1$ to estimate $\langle VT \rangle_{\rm O4a}$ (*solid bars*). $\langle VT \rangle_{\rm O3}$ (*hatched bars*) for each search are shown for reference (Abbott et al. 2023b).

We also report $\langle VT \rangle_{\rm O4a}$ as a function of component masses, $m_{1,2}$, shown in Figure 3 for the same population, and the same per-search detection threshold. We divide the range of component masses, m_1 (m_2) into 5 linearly spaced bins between 0.19 $M_\odot$ to 11.0 (1.1) $M_\odot$. The detected simulated signals are then reweighted to the desired population $\mathbf{\Lambda}$ using Equation (A2) to compute the $\langle VT \rangle$ within each bin. We observe similar trends in this case for the individual searches: the ratio of $\langle VT \rangle_{\rm O4a}$ to $\langle VT \rangle_{\rm O3}$ averaged across all bins is 1.2, 1.0, and 1.4 for GstLAL, MBTA, and PyCBC respectively.

3.2. *Sub-solar mass BNS*

Following the search sensitivity as reported in Abac et al. (2025a), we compute the sensitive hypervolume for BNS systems at representative combinations of component masses for two distinct cases extending into the low-mass NS parameter space:

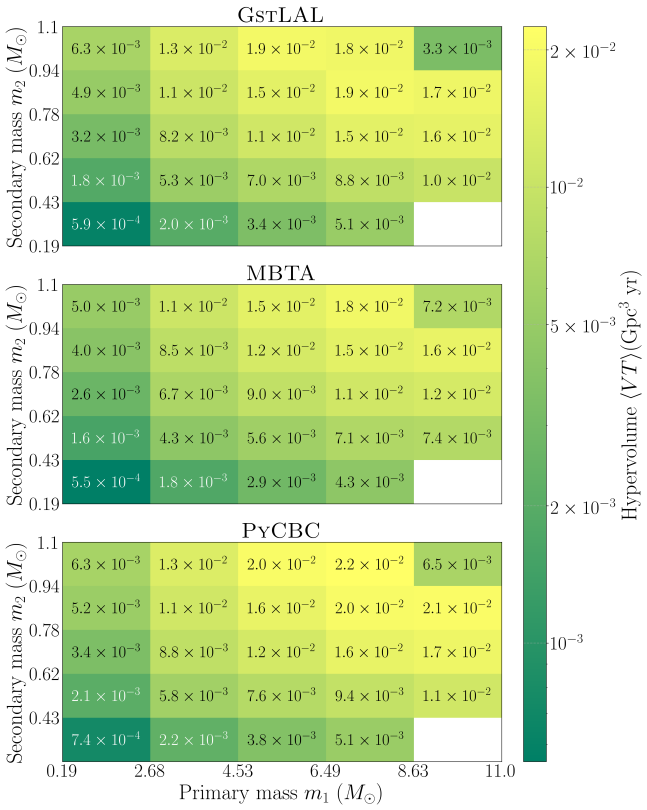

Figure 3. The sensitive hypervolume, $\langle VT \rangle$ as a function of the component masses, (m_1, m_2), computed for searches GstLAL, MBTA and PyCBC following the injection campaign in data from O4a. The color of each cell corresponds to the $\langle VT \rangle_{\rm O4a}$ value. The sources within each bin are reweighted to a log-uniform distribution with 0.19 $M_\odot \leq m_2 \leq 1.1\,M_\odot$ and $m_2 \leq m_1 \leq 11.1\,M_\odot$ with $q \geq 0.05$, and the spin distribution is reweighted to an isotropic uniform distribution with $\chi_{1,2} \leq 0.1$ to estimate $\langle VT \rangle_{\rm O4a}$.

- Double SSM: $m_{1,2} \leq 1\,M_\odot$. We pick three combinations with $m_{1,2}$ equal to 0.6 $M_\odot$, 0.8 $M_\odot$, and 1 $M_\odot$ with $m_2 \leq m_1$.
- Single SSM: $m_1 > 1\,M_\odot$ while $m_2 \leq 1\,M_\odot$. We pick combinations of m_1 equal to 1.4 $M_\odot$, 1.8 $M_\odot$, and 2.2 $M_\odot$ with m_2 equal to 0.6 $M_\odot$, 0.8 $M_\odot$, and 1 $M_\odot$.

The primary difference in the considered BNS populations compared to analyses reported in Abac et al. (2025a,e) is the extension of the NS mass distributions down to 0.5 $M_\odot$. Unlike the BBH case, we compute the sensitive hypervolume at each point by reweighting the injections to a log-normal distribution about the central mass with a width of 0.1. Therefore, 0.6 $M_\odot$ is the lowest central mass we consider to avoid regions of the parameter space with no injections. For each point in the component mass parameter space, we assume an

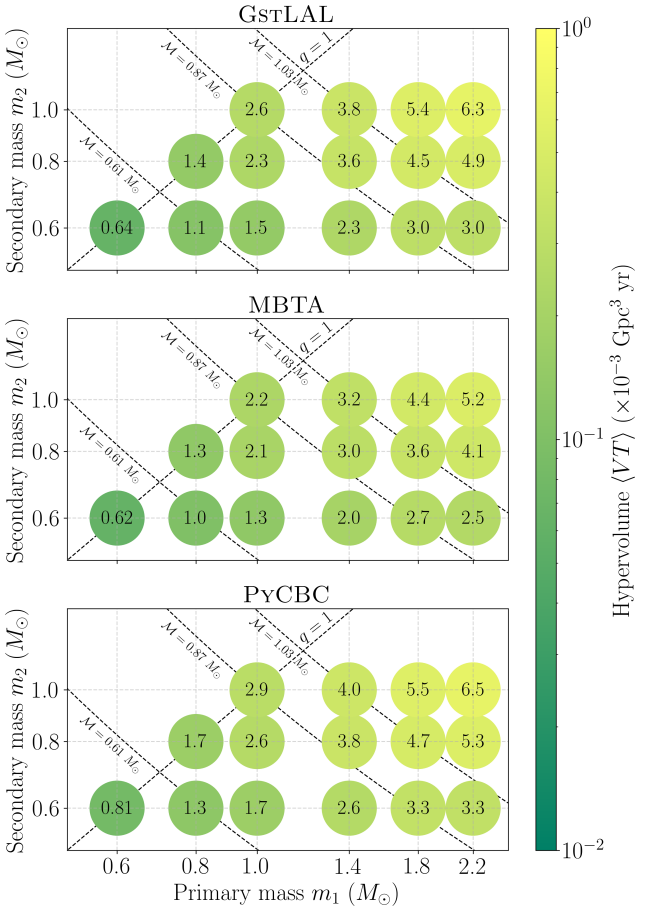

Figure 4. The sensitive hypervolume, $\langle VT \rangle$ (Gpc^3 yr) for a high-spinning BNS population applying a significance threshold FAR $\leq$ 1 yr^{-1}. We report the $\langle VT \rangle_{\rm O4a}$ for GstLAL, MBTA and PyCBC computed using Equation (1). The color of each circle corresponds to the $\langle VT \rangle_{\rm O4a}$ value. The plotted points correspond to the central points of log-normal distributions with widths 0.1 used to estimate $\langle VT \rangle_{\rm O4a}$.

isotropic distribution of spins with spin magnitudes $\chi_{1,2} \leq 0.4$. Figure 4 shows the resulting variation in $\langle VT \rangle_{\rm O4a}$ with a detection threshold of FAR ≤ 1 yr^{-1} for each search following the detection threshold used for computing $\langle VT \rangle$ in Abac et al. (2025a).

We also find that the search sensitivity is largely agnostic to different mass models for NS like the PEAK and POWER models constrained using data from GWTC-4.0 (Abac et al. 2025e) with $\langle VT \rangle_{\rm O4a}$ comparable to the estimates shown in Figure 4.

The 1σ statistical uncertainty on $\langle VT \rangle$ arising from the finite number of samples used to estimate $\xi(\mathbf{\Lambda})$ (Equation 2) ranges between 2%–8% for BBHs and 2%–10% for BNSs. Sources of systematic uncertainty include but are not limited to calibration errors and waveform systematics. The median calibration error in O4a is estimated to be at the percent level (Abac et al. 2025b) resulting in systematic uncertainties $< 10\%$ in $\langle VT \rangle$. Waveform systematics from extrapolation of tidal effects for sub-solar mass BNS are not fully understood in this sub-solar mass regime. Further, numerical relativity simulations used to calibrate waveform models including tidal effects do not cover the low masses and large radii relevant to this regime. For considered BBH, waveform systematics are sub-dominant to statistical errors. Given the bandwidth of present searches largely covers the inspiral, effects from modeling uncertainties at merger and ringdown are expected to be minimal.

4. RATES

Assuming a Poisson rate for triggers produced by the searches, we use the loudest event statistic formalism (Biswas et al. 2009) to derive the upper limit on the merger rate for the population of SSM BBHs considered in this work. Since the most significant events in the three participating search pipelines are consistent with background with the exception of GW230529_181500 which is conclusively known to have super-solar masses (Abac et al. 2024b), we derive the upper limit on the merger rate at the 90% confidence level, $\mathcal{R}_{90,i}$ using $\langle VT \rangle_{\rm O4a}$ as follows:

$$\mathcal{R}_{90,i} = \frac{2.3}{\langle VT \rangle_i}, \tag{4}$$

where the $\mathcal{R}_{90,i}$ is computed in the corresponding i–th mass bin (Biswas et al. 2009).

Figure 5 shows the upper limit on the merger rate at the 90% confidence level for GstLAL, MBTA, and PyCBC as a function of the chirp mass $\mathcal{M}$. Since $\mathcal{R}_{90,i}$ is derived through a rescaling of the $\langle VT \rangle_i$, we find that using data from O4a alone yields only marginal improvement relative to O3. We find the most constraining limit on $\mathcal{R}_{90}^{\rm O4a}$ to be $(127 \pm 3)\,{\rm Gpc}^{-3}\,{\rm yr}^{-1}$,

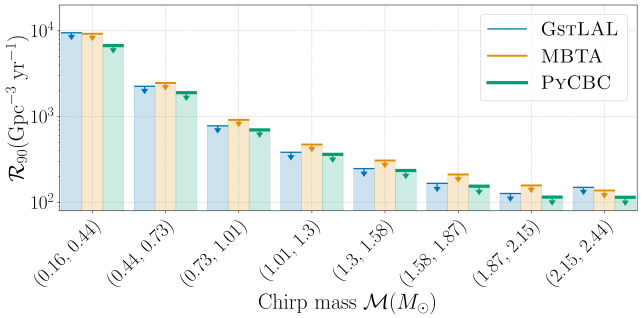

Figure 5. Upper limits on the merger rate of SSM BBH at the 90% confidence level, $\mathcal{R}_{90}^{\rm O4a}$ (Gpc^{-3} yr^{-1}), at the end of O4a as a function of the chirp mass $\mathcal{M}$ for search pipelines GstLAL (*blue*), MBTA (*yellow*) and PyCBC (*green*). The upper limits are computed following Equation 4 using the estimated $\langle VT \rangle$ within chirp mass bins specified along the x-axis. The arrows point in the direction of possible merger rates informed by $\langle VT \rangle_{\rm O4a}$ for each search.

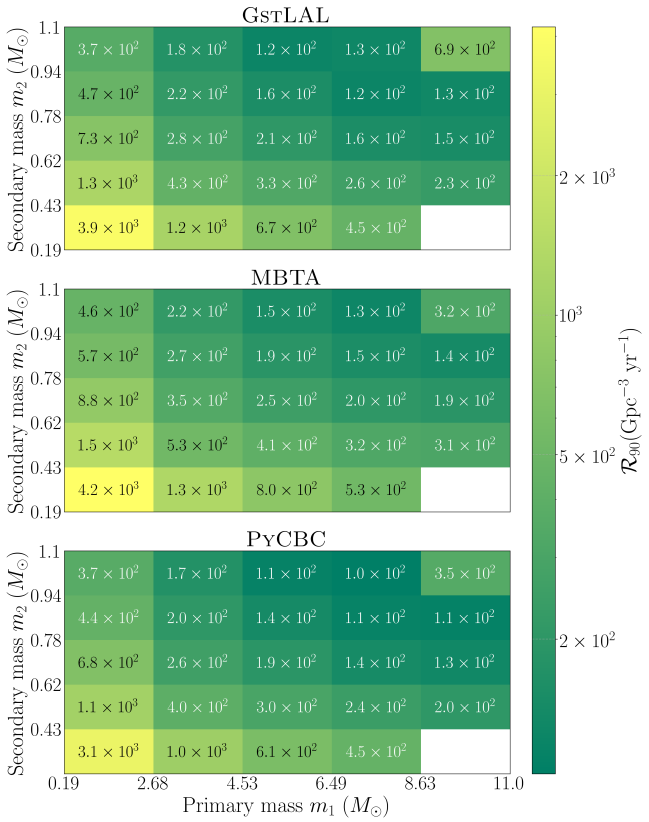

Figure 6. Upper limits on the merger rate of SSM BBH at the 90% confidence interval, $\mathcal{R}_{90}$ (Gpc^{-3} yr^{-1}) as a function of the component masses, (m_1, m_2), computed for searches GstLAL, MBTA and PyCBC. The color of each cell corresponds to the $\mathcal{R}_{90}^{\mathrm{O4a}}$ calculated using Equation 4 with $\langle VT \rangle_{\mathrm{O4a}}$ shown in Figure 3.

(138 ± 4) Gpc^{-3} yr^{-1}, and (115 ± 3) Gpc^{-3} yr^{-1}for GstLAL, MBTA, and PyCBC respectively.

We also report upper limits on $\mathcal{R}_{90}^{\mathrm{O4a}}$ as a function of (m_1, m_2) as shown in Figure 6. Following the binning in the $m_{1,2}$ parameter space described in Section 3.1, $\mathcal{R}_{90,i}^{\mathrm{O4a}}$ are computed using Equation (4) in each bin. We find the most constraining limit on $\mathcal{R}_{90}^{\mathrm{O4a}}$ to be (122 ± 5) Gpc^{-3} yr^{-1}, (126 ± 5) Gpc^{-3} yr^{-1}, and (102 ± 4) Gpc^{-3} yr^{-1}for GstLAL, MBTA, and PyCBC respectively.

Here, we have included the 1σ uncertainties when quoting the most constraining rate upper limit. Propagating the $\langle VT \rangle_{\mathrm{O4a}}$ uncertainty (Equation 2) expectedly yields 1σ statistical errors on the BBH merger rate upper limits between 2% and 8%. Note that systematic uncertainties on $\langle VT \rangle_{\mathrm{O4a}}$ result in equivalent uncertainties on the rate upper limits.

Similar to the estimation of the merger rate for BNS assuming a simple, fixed population in Abac et al. (2025e), we estimate the merger rate for SSM BNSs. Following the SIMPLE UNIFORM BNS model with modifications to the range of component masses, we assume a uniform mass distribution between 0.5 $M_\odot$ and 2.5 $M_\odot$ for m_1, and a uniform mass distribution between 0.5 $M_\odot$ and 1 $M_\odot$ for m_2 with $m_2 \leq m_1$, isotropically distributed spins with uniform spin magnitudes below 0.4, and a merger rate uniform in comoving volume up to $z_{\mathrm{max}} = 0.2$. Under this fiducial model with zero SSM-BNS detections for a FAR threshold of 2 yr^{-1}, we find the upper limit at the 90% confidence level to be 86 Gpc^{-3} yr^{-1}. Although the merger rate we estimate is broadly consistent with the reported rate for the SIMPLE UNIFORM BNS model in Abac et al. (2025e), the two are not directly comparable due to the differences in assumptions about the underlying BNS populations.

5. CONSTRAINING DARK MATTER

The upper limits on merger rates derived in Section 4 can be cast into constraints on any model that predicts an observable number of binary mergers within the considered sub-solar mass search parameter space. In this work we consider two possible sources of BBH mergers, PBHs in Section 5.1 and DBHs in Section 5.2. For each model, we present the constraints in terms of the maximum fraction of dark matter allowed by our observations that can be composed of BHs below a solar mass.

5.1. *Primordial Black Holes*

In the literature, numerous PBH models have been proposed (Carr et al. 2024; Bagui et al. 2025), each predicting a different PBH abundance characterized by the fraction of the dark matter cosmological density composed of PBHs, defined as $f_{\mathrm{PBH}} = \rho_{\mathrm{PBH}}/\rho_{\mathrm{DM}}$, where ρ_{PBH} and ρ_{DM} are the present-day mass densities of PBHs and dark matter, respectively. Constraining f_{PBH} robustly using GW observations is challenging because, for a given f_{PBH}, the predicted binary merger rates at the present epoch vary significantly across models. These variations primarily arise from differences in the initial mass distributions and clustering properties of PBHs. Moreover, the merger rate predictions remain highly uncertain as they are strongly influenced by complex phenomena such as many-body interactions and non-linear gravitational effects, which are difficult to model accurately.

PBH binaries are typically considered to form in two scenarios, early binaries (EB) and late binaries (LB). Early binaries form shortly after PBH formation as pairs of PBHs decouple from the Universe's expansion and form eccentric binaries through tidal interactions with nearby PBHs (Nakamura et al. 1997). Consequently, merger rates of early binaries are strongly influenced by initial PBH clustering and mass distribution. In contrast, late binaries form in dense halos through dynamical interactions, with merger rates shaped by local density and halo properties (Siles & García-Bellido Capdevila 2025).

We model the merger rate of early binaries as in Abbott et al. (2023b), using the analytical approximations developed

in Hütsi et al. (2021); Vaskonen & Veermäe (2020); Chen & Huang (2018); Ali-Haïmoud et al. (2017) and validated by N-body simulations in Raidal et al. (2019) [1]:

$$\frac{\mathrm{d}^2\mathcal{R}^{\rm PBH}_{\rm EB}}{\mathrm{d}\ln m_A \mathrm{d}\ln m_B} = 1.6\times10^6\,\mathrm{Gpc^{-3}\,yr^{-1}} \times f_{\rm sup} f_{\rm PBH}^{53/37} f(\ln m_A) \times f(\ln m_B)\left(\frac{m_A+m_B}{M_\odot}\right)^{-32/37}\left[\frac{m_A m_B}{(m_A+m_B)^2}\right]^{-34/37}, \quad (5)$$

where m_A and m_B denote the component masses of the PBH binary, without imposing any ordering between them, in contrast to the convention $m_1 \geq m_2$ used elsewhere in this work. $f(\ln m)$ is the normalized PBH mass function (i.e., the probability density over $\ln m$), and $f_{\rm sup}$ is a suppression factor that accounts for binary disruption due to gravitational interactions with other PBHs or surrounding matter. To remain consistent with Abbott et al. (2023b), we adopt $f_{\rm sup} = 2.3\times10^{-3} f_{\rm PBH}^{-0.65}$ throughout this work, representative of a high-suppression scenario (Hütsi et al. 2021), and thus leading to conservative constraints.

The merger rate of late binaries is significantly more challenging to model, as this channel involves complex dynamical interactions. Following Clesse & García-Bellido (2022); Phukon et al. (2021), we assume

$$\frac{\mathrm{d}^2\mathcal{R}^{\rm PBH}_{\rm LB}}{\mathrm{d}\ln m_A \mathrm{d}\ln m_B} = R_{\rm clust} f_{\rm PBH} f(\ln m_A) f(\ln m_B) \frac{(m_A+m_B)^{10/7}}{(m_A m_B)^{5/7}}, \quad (6)$$

where $R_{\rm clust}$ is a scaling factor that depends on the PBH clustering properties, including their velocity distribution. While there is general agreement on the mass dependence of the late binaries' merger rate (e.g., Bird et al. 2016), the overall amplitude remains highly uncertain due to its strong sensitivity to the underlying clustering scenario. As in Clesse & García-Bellido (2022); Phukon et al. (2021), we assume $R_{\rm clust} = 420\,\mathrm{Gpc^{-3}\,yr^{-1}}$, noting that this represents a high clustering scenario, and constraints derived under this assumption are therefore conservative.

We use the theoretical merger rate models of Equations (5, 6) to set upper limits on $f_{\rm PBH}$, assuming a point PBH mass distribution, i.e., $f(\ln m) = \delta(\ln m - \ln m_{\rm PBH})$. The limits are obtained by identifying the value of $f_{\rm PBH}$ for which the theoretical rates match the 90% confidence level upper bounds on merger rates derived using Equation (4).

[1] The merger-rate expression in Eq. (5), while widely used in the literature, is validated using N-body simulations in a limited region of parameter space. In particular, the simulations of Raidal et al. (2019) consider $\sim O(10^2)$ equal-mass $\sim 30, M_\odot$ PBHs with $f_{\rm PBH} \lesssim 0.1$, which differs significantly from the lower masses and larger PBH abundances explored here.

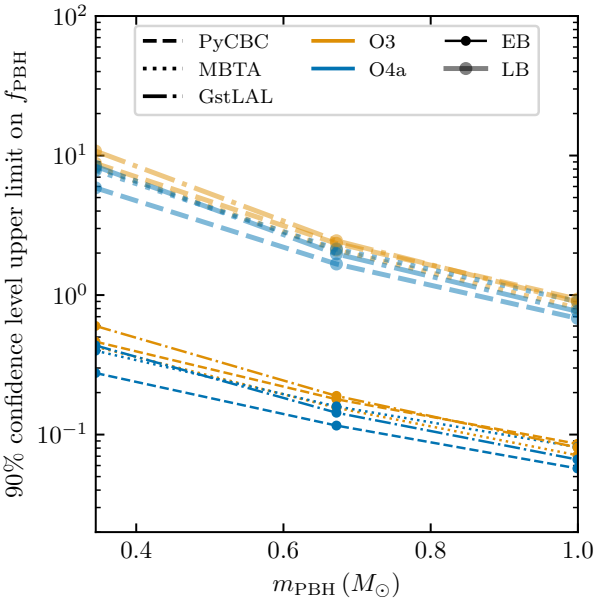

Figure 7. Upper limits on the PBH dark matter fraction $f_{\rm PBH}$ as a function of PBH mass $m_{\rm PBH}$. Constraints are derived using the merger rate models given by Equation (5) for early binaries (EB), and Equation (6) for late binaries (LB), assuming a a point mass function. Results are shown at the 90% confidence level using the sensitive hypervolumes $\langle VT\rangle$ calculated for GstLAL, MBTA, and PyCBC during O3 and O4a.

Figure 7 shows the resulting constraints for both early binaries and late binaries, using the $\langle VT\rangle$ of the GstLAL, MBTA, and PyCBC pipelines in O3 and O4a. We find close agreement among the different pipelines. The constraints from O3 and O4a are of similar magnitude, reflecting the comparable $\langle VT\rangle$s in the two observing runs, though O4a consistently provides slightly stronger limits. These direct search constraints are complementary to the bounds derived from the non-observation of a stochastic GW background from inspiralling SSM PBH binaries at high redshift (Boybeyi et al. 2025; Abac et al. 2025f).

While the constraints presented above assume a point PBH mass function, this is not realistic in most early-formation scenarios (Carr et al. 2024). PBHs are generally expected to form with broad and non-trivial mass distributions (Bagui et al. 2025). To remain agnostic about the specific shape of the mass function, we instead constrain the quantity

$$F_{\rm PBH} = \frac{f_{\rm sup}}{2.3\times10^{-3}} f_{\rm PBH}^{53/37} f(\ln m_A) f(\ln m_B) = f_{\rm PBH}^{0.78} f(\ln m_A) f(\ln m_B), \quad (7)$$

which encapsulates the dependence of the merger rate of early binaries on both the PBH abundance $f_{\rm PBH}$, and the underlying mass distribution $f(\ln m)$. The definition of $F_{\rm PBH}$

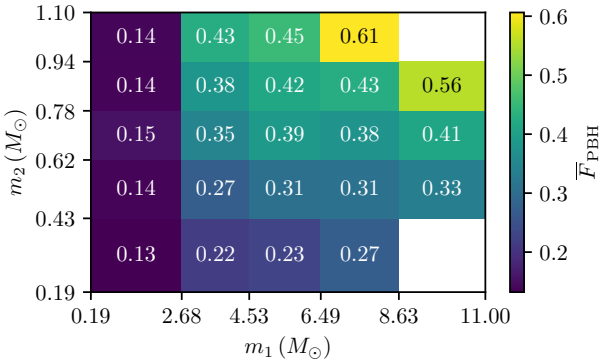

Figure 8. Upper limits on $\overline{F}_{\rm PBH}$ (Equation (7)) as a function of the PBH binary component masses m_1 and m_2. Constraints are derived using the early binary merger rate model of Equation (8). We show the median 90% upper limit across GstLAL, MBTA, and PyCBC calculated using their sensitive hypervolumes $\langle VT\rangle$ in O4a.

explicitly incorporates the assumption $f_{\rm sup} = 2.3\times10^{-3} f_{\rm PBH}^{-0.65}$ adopted throughout this work.

Limits on $F_{\rm PBH}$ are determined by finding the value for which the theoretical merger rate for early binaries matches the 90% confidence level upper bounds derived from Equation (4). We constrain $F_{\rm PBH}$ only for early binaries, since its definition in Equation (7) is specific to this scenario, and merger rate models for late binaries are more uncertain and less constraining. We adopt the binning in (m_1, m_2) from Section 4, and write the integral in Equation (5) within each bin as

$$\mathcal{R}^{\rm PBH}_{\rm EB} = 3.68\times10^3\,{\rm Gpc^{-3}\,yr^{-1}}\,\overline{F}_{\rm PBH}\times\left(\frac{\overline{m}_1+\overline{m}_2}{M_\odot}\right)^{-32/37} \times\left[\frac{\overline{m}_1\overline{m}_2}{(\overline{m}_1+\overline{m}_2)^2}\right]^{-34/37}\ln\left(\frac{m_1^{\rm max}}{m_1^{\rm min}}\right)\ln\left(\frac{m_2^{\rm max}}{m_2^{\rm min}}\right), \quad (8)$$

where $m_{1,2}^{\rm min}$ and $m_{1,2}^{\rm max}$ denote the bin edges for the component masses, $\overline{m}_{1,2} = (m_{1,2}^{\rm min}+m_{1,2}^{\rm max})/2$ is the central value, and $\overline{F}_{\rm PBH}$ denotes the effective bin-averaged value of $F_{\rm PBH}$, defined implicitly such that Eq. (8) reproduces the exact integral of the merger rate over the bin.

Figure 8 shows the median 90% upper limit on $\overline{F}_{\rm PBH}$ across all search pipelines, based on the results from O4a. We find that $\overline{F}_{\rm PBH}$ is constrained to be less than unity across the entire range of (m_1, m_2) explored in this work, though the limits remain relatively weak as they lie close to unity.

5.2. *Dissipative Dark Matter*

Dissipative dark matter is a class of models which posit that dark matter may have complex particle interactions similar to those of the Standard Model, including dissipative processes. Whenever there is a fermion in the model, dark matter has a Chandrasekhar limit analogous to that of the Standard Model, but with a value that depends on the dark matter particle mass(es) (Mohapatra & Teplitz 1999; D'Amico et al. 2018; Shandera et al. 2018; Choquette et al. 2019; Chang et al. 2019; Bramante et al. 2024). In dissipative scenarios, particle interactions allow energy to be transported away from gravitationally bound systems such as dark matter halos. These dissipative interactions become more efficient in denser regions, and some dense regions may dissipate energy efficiently enough for gravity to dominate, leading to the formation of ultra-compact objects made of dark matter. When those are sufficiently massive, above the dark Chandrasekhar limit, they are dark black holes. Therefore, GW signals from DBH binaries provide a way to probe the microphysics of dissipative dark matter even if it is not coupled to the Standard Model beyond gravity, or if the coupling is too weak to be detectable in the near future.

Although the fragmentation scale of the dark gas depends on the chemistry of the dark sector, the dynamical processes that lead to the formation of compact objects are analogous to those in star formation. While simulation of such small-scale phenomena in novel dark matter scenarios remains challenging, it is reasonable to expect that the initial mass function and binary fraction of DBHs are qualitatively similar to that of baryonic objects. For the particular worked example of atomic dark matter (Ackerman et al. 2009; Kaplan et al. 2011; Cyr-Racine & Sigurdson 2013), where cooling and compact object formation has been extensively studied (Rosenberg & Fan 2017; Ryan et al. 2022a; Gurian et al. 2022; Ryan et al. 2022b), there is a close parallel between DBH formation and Population III star formation that further supports this statement. Thus, we use a truncated power-law mass model characterized by a minimum mass $M_{\rm min}$, power $-b$, and ratio of maximum mass to minimum mass $r = M_{\rm max}/M_{\rm min}$, and assume a binary fraction of $f_{\rm binary} = 0.26$ (Shandera et al. 2018) in our analysis. The total number of DBHs in this population is set by $f_{\rm DBH} \equiv \rho_{\rm DBH}/\rho_{\rm DM}$ where $\rho_{\rm DBH}$ and $\rho_{\rm DM}$ are the densities of DBHs and dark matter, respectively. The rate of DBH binaries merging in this population, $\mathcal{R}$, is computed as (Singh et al. 2021)

$$\frac{{\rm d}\mathcal{R}(\mathcal{M}\mid f_{\rm DBH},\theta)}{{\rm d}\mathcal{M}} = \Big[p(\mathcal{M}\mid t_m,\theta)\times p(t_m\mid\theta)\Big]_{t_m=10\,{\rm Gyr}} \times\left(\frac{\rho_{\rm DM}\times f_{\rm DBH}\times f_{\rm binary}}{\langle M\rangle}\right), \quad (9)$$

where $p(\mathcal{M}\mid t_m,\theta)$ is the distribution of $\mathcal{M}$ with a time of merging t_m, $p(t_m\mid\theta)$ is the probability distribution of times-to-merger (these two factors evaluated at $t_m = 10\,{\rm Gyr}$), $\rho_{\rm DM} = 3.3\times10^{19}\,M_\odot\,{\rm Gpc^{-3}}$, and $\langle M\rangle$ is the average component mass of the DBH binaries. The merger times are calcu-

lated using Peters formula for coalescing binaries (Peters & Mathews 1963).

We use a Bayesian analysis to constrain this population of DBHs by creating $\mathcal{M}$ bins and modeling the number of detected binaries in each bin using a Poisson distribution. With the non-detection of SSM events, the likelihood in the i–th chirp-mass bin is $P(0|\mathcal{R}_i, \langle VT\rangle_i, \mathcal{M}) = e^{-\mathcal{R}_i\langle VT\rangle_i}$, where the rate $\mathcal{R}_i$ is determined by integrating Equation (9) over the width of the i–th $\mathcal{M}$ bin, and the sensitive hypervolume VT_i is informed by this SSM search. To maintain a consistent null-detection result in every $\mathcal{M}$ bin, we adopt a more stringent FAR threshold of 0.01 yr^{-1} when estimating the pipeline-specific $\langle VT\rangle_{\rm O4a}$ for this analysis. We use priors consistent with previous analyses (Abbott et al. 2022, 2023b): uniform priors on $M_{\rm min}$ over the interval $[10^{-3}\,M_\odot, 3.1\,M_\odot]$, b over the interval $[-1, 2]$, and $f_{\rm DBH}$ over the interval $[10^{-10}, 1]$, and a log-uniform prior on r over the interval $[2, 1000]$. Bayes' law then states the log-posterior is

$$\ln p(f_{\rm DBH}, M_{\rm min}, r, b) = -\sum_i \mathcal{R}_i(f_{\rm DBH}, M_{\rm min}, r, b)\langle VT\rangle_i - \ln r + C, \tag{10}$$

where C is the normalization constant.

Previous analyses evaluated the posterior distribution using a grid-based method (Abbott et al. 2022, 2023b), while we use the MCMC sampler EMCEE (Foreman-Mackey et al. 2013) to explore the parameter space for faster convergence in this analysis. We marginalize over r and b to constrain $f_{\rm DBH}$ and $M_{\rm min}$. Figure 9 shows the two-dimensional PDF of $f_{\rm DBH}$ and $M_{\rm min}$ derived from $\langle VT\rangle_{\rm O4a}$ for GstLAL, MBTA, and PyCBC individually. Given no detections, the resulting posterior distribution can be interpreted as upper limits on $f_{\rm DBH}$.

The exclusion region in the $f_{\rm DBH}$–$M_{\rm min}$ space extends as low as $f_{\rm DBH} = (1.2\,\text{to}\,1.3)\times10^{-5}$ at $M_{\rm min} = 1\,M_\odot$, where the range arises from the differing sensitivities of the search pipelines. This limit on $f_{\rm DBH}$ is consistent with the dissipative dark matter scenario as the formation channel requires efficient cooling, which only occurs in regions dense in dark matter. Since we restrict our prior on $r \leq 1000$, a non-detection provides no information below $0.020\,M_\odot - 0.021\,M_\odot$ because the searches have minimal support for mass distributions with lower minimum masses. Additionally, we exclude limits where $M_{\rm min} > 1\,M_\odot$ as an SSM detection necessitates the minimum mass to be smaller than $1\,M_\odot$. The range of dark fermion masses m_χ probed by this search is set by $M_{\rm min}$ via dark Chandrasekhar mass, $M^{\rm Dark}_{\rm Chandra} \propto M^3_{\rm Planck}/(\mu^{\rm Dark} m_\chi)^2 \leq M_{\rm min}$, where $\mu^{\rm Dark} m_\chi$ is the mass per degenerate fermion (Chandrasekhar 1931). We derive a bound on the ratio of m_χ to the mass of the Standard Model proton m_p by taking the ratio of the stellar Chandrasekhar mass to the dark Chandrasekhar mass as

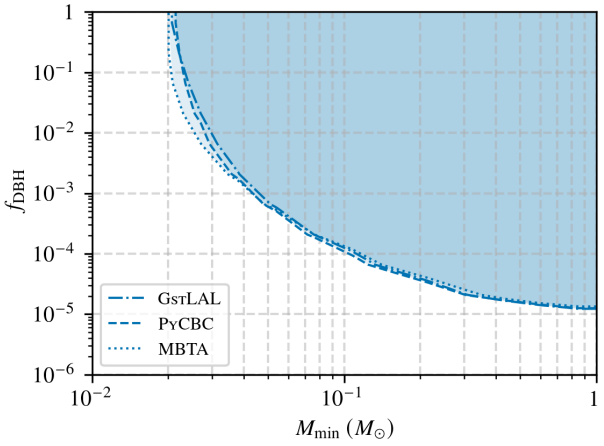

Figure 9. Contours in the $f_{\rm DBH}$–$M_{\rm min}$ plane for the atomic dark matter model after marginalizing over the ratio of maximum to minimum mass, and the slope of the black hole population. Using the two-dimensional PDF $p(f_{\rm DBH}, M_{\rm min})$, we calculate 90% of the posterior mass to be outside of the shaded region. Constraints shown are derived from $\langle VT\rangle_{\rm O4a}$ for the GstLAL, MBTA, and PyCBC pipelines evaluated with a FAR threshold of 0.01 yr^{-1}.

$$\mu^{\rm Dark}\frac{m_\chi}{m_p} = 2\sqrt{\frac{1.4\,M_\odot}{M^{\rm Dark}_{\rm Chandra}}} \leq 2\sqrt{\frac{1.4\,M_\odot}{M_{\rm min}}}, \tag{11}$$

where we have set the stellar Chandrasekhar mass to $1.4\,M_\odot$, and corresponding $\mu^{\rm Stellar}$ to 2.

Previous searches (Abbott et al. 2023b) used the Standard Model value of $\mu^{\rm Dark} = 2$, but we report the bound leaving $\mu^{\rm Dark}$ unspecified to cover a broader range of dissipative dark matter models. The search thus probed $\mu^{\rm Dark} m_\chi/m_p$ in the range $2.4 < \mu^{\rm Dark} m_\chi/m_p < 16.1 - 16.7$ where the range arises from the differing sensitivities of the search pipelines. A future detection would be able to put a direct bound on the microphysics of dissipative dark matter.

6. CONCLUSION

We present results from SSM searches for compact objects in data from the first part of the fourth LIGO–Virgo–KAGRA observing run O4a. No significant candidate, other than the previously published candidate GW230529_181500 (Abac et al. 2024b), is reported by the three participating searches. Although all searches detect GW230529_181500, it is excluded as a possible SSM detection because the component masses of the source binary are reliably known to be greater than a solar mass. Given the null detection result, we report upper limits on the merger rates for SSM BBHs with masses greater than $0.2\,M_\odot$ using the estimated search sensitivity.

Using the inferred sensitive hypervolume and limits on the merger rate of SSM BBHs, we update the constraints on two dark matter models: PBHs, and DBHs that form in a dissipative dark matter model. While both models can popu-

late the sub-solar and super-solar regime, we turn to the SSM parameter space for clear evidence of such objects because no known astrophysical channel produces SSM black holes. O4a data alone provides only marginal improvement over previous limits (Abbott et al. 2023b).

The sensitive hypervolume is subject to both statistical and systematic uncertainties that directly influence the resulting merger rate upper limits and constraints on dark matter models. Statistical uncertainty from the finite injection sampling is compounded by effects like calibration errors, and waveform systematics. We adopt a more conservative, binned approach to report the sensitivity of searches ensuring the limits remain robust against sampling fluctuations.

In the PBH scenario, we set informative constraints on the fraction of dark matter in PBHs $f_{\rm PBH}$ in late-forming binaries for the first time, with $f_{\rm PBH} < 1$ at the 90% C.L. for $m_{\rm PBH} \gtrsim 0.9\,M_\odot$ using the $\langle VT \rangle$ from O4a. For early-forming PBH binaries, we obtain the strongest constraints from gravitational wave observations to date, with $f_{\rm PBH}$ upper limits between 0.4 and 0.07 over the range of PBH masses probed by this search. For the dissipative dark matter scenario, we find that SSM DBHs can only form $(1.2\,\text{to}\,1.3) \times 10^{-5}$ of the total dark matter density in the Universe.

For the first time, we report the sensitivity of SSM searches to binaries containing low-mass neutron stars. We find that the typical sensitive hypervolume is $\langle VT \rangle \sim 10^{-3}\,\mathrm{Gpc}^3\,\mathrm{yr}$ for populations of BNSs with at least one SSM neutron star. These searches can also provide insight into matter at high densities given the overlap of the neutron star and SSM parameter space, serving as motivation for low-latency SSM searches (Alléné et al. 2025; Hanna et al. 2025) which started to release alerts in early 2025.

Recently, Kacanja et al. (2026) reported results from an SSM search that includes tidal effects for low mass neutron stars covering binaries with $0.1\,M_\odot \leq m_1(m_2) \leq 2\,M_\odot (1\,M_\odot)$, and aligned spins $-0.05 \leq \chi_{1,2} \leq 0.05$. They report no significant candidate from this search, and find consistent limits on the merger rate for overlapping regions of the parameter space.

The LIGO detectors resumed observation with improved sensitivity, and were joined by the Virgo detector in the second part of the fourth observing run (O4b), and by the KAGRA detector in the third part of the fourth observing run (O4c). With increased observing time as we include data from the later parts of the fourth observing run, we expect the search sensitivity to increase by a factor of 2–3 leading to improved constraints on the merger rate of SSM BBHs. These advances will provide more stringent limits on the fraction of dark matter in SSM compact objects, or perhaps even detect a gravitational wave signal originating from the merger of SSM compact objects. Such a detection would have deep implications for fundamental physics.

DATA AVAILABILITY

All strain data analysed as part of this publication are publicly available through Gravitational Wave Open Science Center (GWOSC). The details of this data release are described in detail in Abac et al. (2025b). Associated data release includes trigger files for candidates reported in Table 1, BBH sensitive volume-time, and injection results used in the calculation of sensitive volume-time reported in this paper (LIGO–Virgo–KAGRA Collaboration 2026).

ACKNOWLEDGEMENTS

This material is based upon work supported by NSF's LIGO Laboratory, which is a major facility fully funded by the National Science Foundation. The authors also gratefully acknowledge the support of the Science and Technology Facilities Council (STFC) of the United Kingdom, the Max-Planck-Society (MPS), and the State of Niedersachsen/Germany for support of the construction of Advanced LIGO and construction and operation of the GEO 600 detector. Additional support for Advanced LIGO was provided by the Australian Research Council. The authors gratefully acknowledge the Italian Istituto Nazionale di Fisica Nucleare (INFN), the French Centre National de la Recherche Scientifique (CNRS) and the Netherlands Organization for Scientific Research (NWO) for the construction and operation of the Virgo detector and the creation and support of the EGO consortium. The authors also gratefully acknowledge research support from these agencies as well as by the Council of Scientific and Industrial Research of India, the Department of Science and Technology, India, the Science & Engineering Research Board (SERB), India, the Ministry of Human Resource Development, India, the Spanish Agencia Estatal de Investigación (AEI), the Spanish Ministerio de Ciencia, Innovación y Universidades, the European Union NextGenerationEU/PRTR (PRTR-C17.I1), the ICSC - CentroNazionale di Ricerca in High Performance Computing, Big Data and Quantum Computing, funded by the European Union NextGenerationEU, the Comunitat Autonòma de les Illes Balears through the Conselleria d'Educació i Universitats, the Conselleria d'Innovació, Universitats, Ciència i Societat Digital de la Generalitat Valenciana and the CERCA Programme Generalitat de Catalunya, Spain, the Polish National Agency for Academic Exchange, the National Science Centre of Poland and the European Union - European Regional Development Fund; the Foundation for Polish Science (FNP), the Polish Ministry of Science and Higher Education, the Swiss National Science Foundation (SNSF), the Russian Science Foundation, the European Commission, the European Social Funds (ESF), the European Regional Development Funds (ERDF), the Royal Society, the Scottish Funding Council, the Scottish Universities Physics Alliance, the Hungarian Scientific Research Fund (OTKA), the French

Lyon Institute of Origins (LIO), the Belgian Fonds de la Recherche Scientifique (FRS-FNRS), Actions de Recherche Concertées (ARC) and Fonds Wetenschappelijk Onderzoek - Vlaanderen (FWO), Belgium, the Paris Île-de-France Region, the National Research, Development and Innovation Office of Hungary (NKFIH), the National Research Foundation of Korea, the Natural Sciences and Engineering Research Council of Canada (NSERC), the Canadian Foundation for Innovation (CFI), the Brazilian Ministry of Science, Technology, and Innovations, the International Center for Theoretical Physics South American Institute for Fundamental Research (ICTP-SAIFR), the Research Grants Council of Hong Kong, the National Natural Science Foundation of China (NSFC), the Israel Science Foundation (ISF), the US-Israel Binational Science Fund (BSF), the Leverhulme Trust, the Research Corporation, the National Science and Technology Council (NSTC), Taiwan, the United States Department of Energy, and the Kavli Foundation. The authors gratefully acknowledge the support of the NSF, STFC, INFN and CNRS for provision of computational resources.

This work was supported by MEXT, the JSPS Leading-edge Research Infrastructure Program, JSPS Grant-in-Aid for Specially Promoted Research 26000005, JSPS Grant-in-Aid for Scientific Research on Innovative Areas 2402: 24103006, 24103005, and 2905: JP17H06358, JP17H06361 and JP17H06364, JSPS Core-to-Core Program A. Advanced Research Networks, JSPS Grants-in-Aid for Scientific Research (S) 17H06133 and 20H05639, JSPS Grant-in-Aid for Transformative Research Areas (A) 20A203: JP20H05854, the joint research program of the Institute for Cosmic Ray Research, University of Tokyo, the National Research Foundation (NRF), the Computing Infrastructure Project of the Global Science experimental Data hub Center (GSDC) at KISTI, the Korea Astronomy and Space Science Institute (KASI), the Ministry of Science and ICT (MSIT) in Korea, Academia Sinica (AS), the AS Grid Center (ASGC) and the National Science and Technology Council (NSTC) in Taiwan under grants including the Science Vanguard Research Program, the Advanced Technology Center (ATC) of NAOJ, the Mechanical Engineering Center of KEK and Vietnam National Foundation for Science and Technology Development (NAFOSTED) 103.01-2025.147.

Additional acknowledgements for support of individual authors may be found in the following document: `https://dcc.ligo.org/LIGO-M2300033/public`. For the purpose of open access, the authors have applied a Creative Commons Attribution (CC BY) license to any Author Accepted Manuscript version arising. We request that citations to this article use 'A. G. Abac *et al.* (LIGO-Virgo-KAGRA Collaboration), ...' or similar phrasing, depending on journal convention.

Facility: LIGO

Software: Calibration of the LIGO strain data was performed with a GstLAL-based calibration software pipeline (Viets et al. 2018). Data-quality products and event-validation results were computed using the DMT (Zweizig 2006), DQR (LIGO Scientific Collaboration and Virgo Collaboration 2018), DQSEGDB (Fisher et al. 2020), gwdetchar (Urban et al. 2021), hveto (Smith et al. 2011), iDQ (Essick et al. 2020), Omicron (Robinet et al. 2020), PEMCHECK (Helmling-Cornell et al. 2024) and PyhonVirgoTools (Virgo Collaboration 2021) software packages and contributing software tools. Analyses in this catalog relied upon the LALSuite software library (LIGO–Virgo–KAGRA Collaboration 2018; Wette 2020). The detection of the signal candidates and subsequent significance evaluations in this paper were performed with the GstLAL-based inspiral software pipeline (Messick et al. 2017; Sachdev et al. 2019; Hanna et al. 2020; Cannon et al. 2020), with the MBTA pipeline (Adams et al. 2016; Aubin et al. 2021), and with the PyCBC (Usman et al. 2016; Nitz et al. 2017; Davies et al. 2020). Sensitive Hypervolume calculations were performed using GWPopulation (Talbot et al. 2025). Plots were prepared with Matplotlib (Hunter 2007), seaborn (Waskom 2021) and GWpy (Macleod et al. 2021). NumPy (Harris et al. 2020), SciPy (Virtanen et al. 2020) and Pandas (pandas development team 2024) were used in the preparation of the manuscript.

APPENDIX

A. METHODS TO DETERMINE THE SEARCH SENSITIVITY

To quantify the sensitivity towards a population with model parameters $\mathbf{\Lambda}$ that determine the population distribution of masses and spins, we determine the fraction of detectable mergers $\xi(\Lambda)$ as follows:

$$\xi(\mathbf{\Lambda}) = \int p(d|\boldsymbol{\theta}) p(\boldsymbol{\theta}|\mathbf{\Lambda}) p_{\rm det}(d) \mathrm{d}d\mathrm{d}\boldsymbol{\theta}, \tag{A1}$$

where $p(d|\boldsymbol{\theta})$ is the likelihood of the data d given a GW source with parameters $\boldsymbol{\theta}$ (the component mass and spins for the individual source), $p(\boldsymbol{\theta}|\mathbf{\Lambda})$ is the likelihood of this source given the population-model hyperparameters $\mathbf{\Lambda}$, and $p_{\rm det}(d)$ is the probability that

Table 2. Fiducial population of BBH and BNS sources used for determining the sensitive hypervolume $\langle VT \rangle$.

	BBH	BNS
Mass Model	$m_{1,2}^{\alpha}, \alpha = -1$	$m_{1,2}^{\alpha}, \alpha = -1$
	$m_1 \in [0.19\,M_\odot, 11.1\,M_\odot]$	$m_1 \in [0.5\,M_\odot, 3\,M_\odot]$
	$m_2 \in [0.19\,M_\odot, 1.1\,M_\odot]$	$m_2 \in [0.5\,M_\odot, 1.1\,M_\odot]$
Spin Magnitude Model	$w\sqrt{\frac{2}{\pi\sigma^2}}\exp\left(-\frac{\chi_{1,2}^2}{2\sigma^2}\right) + (1-w)\frac{\chi_{1,2}^{\alpha-1}(1-\chi_{1,2})^{\beta-1}}{\mathrm{B}(\alpha,\beta)}$	
	$\mu = 0, \sigma = 0.1, \alpha = 1, \beta = 4, w = 0.5$	
	$\chi_{1,2} \in [0, 1]$	
Waveform Model	IMRPhenomXPHM	IMRPhenomXP_NRTidalv3
Equation of State		GPPVA+DD2

Note—Sources are drawn from the given distributions for component masses $m_{1,2}$, and dimensionless spin magnitudes $\chi_{1,2}$ to perform the searches on augmented O4a data. We assume isotropically distributed spins, i.e. the cosine of the angles between the orbital angular momentum vector and the component spin vectors are distributed uniformly. The sources are distributed uniformly in comoving volume and time up to a maximum redshift $z_{\rm max} = 0.2$. This population is denoted by $\mathbf{\Lambda_0}$ in Equation (A2).

the data d produces a trigger above the detection threshold in a search. In practice, $p_{\rm det}(d)$ is determined by the detection statistic assigned by the search.

The importance sampling approach from Essick & Farr (2022) is adopted to calculate $\xi(\mathbf{\Lambda})$ for various choices of $\mathbf{\Lambda}$. We draw $N_{\rm inj}$ source properties from a fiducial population model described by $\mathbf{\Lambda}_0$, and inject simulated signals drawn from the fiducial population into data from O4a. Subsequently, the searches analyze this data to determine the injection recovery. Since the injections are randomly sampled from $\mathbf{\Lambda}_0$, $\xi(\mathbf{\Lambda})$ can be computed through a Monte Carlo sum over the subset of found detections denoted by the set of GW source parameters $\{\boldsymbol{\theta}\}_{\rm found}$, which pass the chosen detection threshold as follows:

$$\xi(\mathbf{\Lambda}) \approx \frac{1}{N_{\rm inj}} \sum_{\boldsymbol{\theta} \in \{\boldsymbol{\theta}\}_{\rm found}} \frac{p(\boldsymbol{\theta}|\mathbf{\Lambda})}{p(\boldsymbol{\theta}|\mathbf{\Lambda}_0)}, \tag{A2}$$

where $p(\boldsymbol{\theta}|\mathbf{\Lambda}_0)$ denotes the probability of the detected source drawn from the fiducial population ($\mathbf{\Lambda}_0$), while $p(\boldsymbol{\theta}|\mathbf{\Lambda})$ denotes the probability of the detected source given the population distribution of interest ($\mathbf{\Lambda}$). Table 2 summarizes the fiducial population describing the source parameters for simulated signals.

Within each population, the simulated signals were injected 32 s apart. PyCBC and GstLAL filtered the BBH and BNS populations separately resulting in analyzing two streams of simulated data. To analyze the simulated data in a single pass, MBTA shifted the BNS injections by 16 s relative to the BBH simulations before injecting them in strain data, resulting in an effective spacing of 16 s. The reduced spacing verifiably did not have a noticeable effect on the efficiency of the MBTA search.

REFERENCES

Abac, A., Dietrich, T., Buonanno, A., Steinhoff, J., & Ujevic, M. 2024a, Phys. Rev. D, 109, 024062, doi: 10.1103/PhysRevD.109.024062

Abac, A. G., et al. 2024b, Astrophys. J. Lett., 970, L34, doi: 10.3847/2041-8213/ad5beb

—. 2025a. https://arxiv.org/abs/2508.18082

—. 2025b. https://arxiv.org/abs/2508.18079

—. 2025c, Astrophys. J. Lett., 995, L18, doi: 10.3847/2041-8213/ae0c06

—. 2025d. https://arxiv.org/abs/2508.18081

—. 2025e. https://arxiv.org/abs/2508.18083

—. 2025f. https://arxiv.org/abs/2510.26848

Abadie, J., et al. 2012, Astrophys. J., 760, 12, doi: 10.1088/0004-637X/760/1/12

Abbott, B., Abbott, R., Adhikari, R., et al. 2008, Phys. Rev. D, 77, 062002, doi: 10.1103/PhysRevD.77.062002

Abbott, B. P., et al. 2016a, Living Rev. Rel., 19, 1, doi: 10.1007/s41114-020-00026-9

Abbott, B. P., Abbott, R., Abbott, T. D., et al. 2016b, Phys. Rev. Lett., 116, 131103, doi: 10.1103/PhysRevLett.116.131103

Abbott, B. P., et al. 2016c, Phys. Rev. Lett., 116, 061102, doi: 10.1103/PhysRevLett.116.061102

—. 2016d, Phys. Rev. X, 6, 041015, doi: 10.1103/PhysRevX.6.041015

—. 2017, Phys. Rev. Lett., 119, 161101, doi: 10.1103/PhysRevLett.119.161101

—. 2018, Phys. Rev. Lett., 121, 231103, doi: 10.1103/PhysRevLett.121.231103

—. 2019a, Phys. Rev. X, 9, 031040, doi: 10.1103/PhysRevX.9.031040

—. 2019b, Phys. Rev. Lett., 123, 161102, doi: 10.1103/PhysRevLett.123.161102

Abbott, R., et al. 2005, Phys. Rev. D, 72, doi: 10.1103/PhysRevD.72.082002

—. 2021, Phys. Rev. X, 11, 021053, doi: 10.1103/PhysRevX.11.021053

—. 2022, Phys. Rev. Lett., 129, 061104, doi: 10.1103/PhysRevLett.129.061104

—. 2023a, Phys. Rev. X, 13, 041039, doi: 10.1103/PhysRevX.13.041039

—. 2023b, Mon. Not. Roy. Astron. Soc., 524, 5984, doi: 10.1093/mnras/stad588

—. 2024, Phys. Rev. D, 109, 022001, doi: 10.1103/PhysRevD.109.022001

Acernese, F., Agathos, M., Agatsuma, K., et al. 2014, Classical and Quantum Gravity, 32, 024001, doi: 10.1088/0264-9381/32/2/024001

Ackerman, L., Buckley, M. R., Carroll, S. M., & Kamionkowski, M. 2009, Phys. Rev. D, 79, 023519, doi: 10.1103/PhysRevD.79.023519

Adams, T., Buskulic, D., Germain, V., et al. 2016, Class. Quant. Grav., 33, 175012, doi: 10.1088/0264-9381/33/17/175012

Ali-Haïmoud, Y., Kovetz, E. D., & Kamionkowski, M. 2017, Phys. Rev. D, 96, 123523, doi: 10.1103/PhysRevD.96.123523

Allen, B., Anderson, W. G., Brady, P. R., Brown, D. A., & Creighton, J. D. E. 2012, Phys. Rev. D, 85, 122006, doi: 10.1103/PhysRevD.85.122006

Alléné, C., et al. 2025, Class. Quant. Grav., 42, 105009, doi: 10.1088/1361-6382/add234

Aubin, F., et al. 2021, Class. Quant. Grav., 38, 095004, doi: 10.1088/1361-6382/abe913

Bagui, E., et al. 2025, Living Rev. Rel., 28, 1, doi: 10.1007/s41114-024-00053-w

Bandopadhyay, A., Reed, B., Padamata, S., et al. 2023, Phys. Rev. D, 107, 103012, doi: 10.1103/PhysRevD.107.103012

Bhattacharya, S., Dasgupta, B., Laha, R., & Ray, A. 2023, Phys. Rev. Lett., 131, 091401, doi: 10.1103/PhysRevLett.131.091401

Bird, S., Cholis, I., Muñoz, J. B., et al. 2016, Phys. Rev. Lett., 116, 201301, doi: 10.1103/PhysRevLett.116.201301

Biswas, R., Brady, P. R., Creighton, J. D. E., & Fairhurst, S. 2009, Class. Quant. Grav., 26, 175009, doi: 10.1088/0264-9381/26/17/175009

Bohé, A., Shao, L., Taracchini, A., et al. 2017, PhysRevD, 95, doi: 10.1103/PhysRevD.95.044028

Boybeyi, T., Clesse, S., Kuroyanagi, S., & Sakellariadou, M. 2025, Phys. Rev. D, 112, 023551, doi: 10.1103/zphk-3ld9

Boyle, M., Brown, D. A., & Pekowsky, L. 2009, Class.Quant.Grav, 26, doi: 10.1088/0264-9381/26/11/114006

Bramante, J., Diamond, M., & Kim, J. L. 2024, JCAP, 02, 002, doi: 10.1088/1475-7516/2024/02/002

Brown, D., Harry, I., Lundgren, A., & Nitz, A. H. 2012, Phys. Rev. D, 86, 084017, doi: 10.1103/PhysRevD.86.084017

Brown, D. A., Kumar, P., & Nitz, A. H. 2013, Phys. Rev. D, 87, 082004, doi: 10.1103/PhysRevD.87.082004

Buonanno, A., Iyer, B. R., Ochsner, E., Pan, Y., & Sathyaprakash, B. 2009, Phys. Rev. D, 80, 084043, doi: 10.1103/PhysRevD.80.084043

Cannon, K., Hanna, C., & Keppel, D. 2012, Phys. Rev. D, 85, 081504, doi: 10.1103/PhysRevD.85.081504

Cannon, K., Hanna, C., & Peoples, J. 2015. https://arxiv.org/abs/1504.04632

Cannon, K., et al. 2020. https://arxiv.org/abs/2010.05082

Capote, E., Jia, W., Aritomi, N., et al. 2025, Phys. Rev. D, 111, 062002, doi: 10.1103/PhysRevD.111.062002

Carr, B., Clesse, S., García-Bellido, J., Hawkins, M., & Kuhnel, F. 2024, Phys. Rept., 1054, 1, doi: 10.1016/j.physrep.2023.11.005

Carr, B., Clesse, S., García-Bellido, J., & K"uhnel, F. 2021, Phys. Dark Univ., 31, 100755, doi: 10.1016/j.dark.2020.100755

Chandrasekhar, S. 1931, Astrophys. J., 74, 81, doi: 10.1086/143324

Chang, J. H., Egana-Ugrinovic, D., Essig, R., & Kouvaris, C. 2019, JCAP, 03, 036, doi: 10.1088/1475-7516/2019/03/036

Chapline, G. F. 1975, Nature, 253, 251, doi: 10.1038/253251a0

Chen, Y.-X., & Metzger, B. D. 2025, Astrophys. J. Lett., 991, L22, doi: 10.3847/2041-8213/ae045d

Chen, Z.-C., & Huang, Q.-G. 2018, Astrophys. J., 864, 61, doi: 10.3847/1538-4357/aad6e2

Chiba, T., & Yokoyama, S. 2017, PTEP, 2017, 083E01, doi: 10.1093/ptep/ptx087

Choquette, J., Cline, J. M., & Cornell, J. M. 2019, JCAP, 07, 036, doi: 10.1088/1475-7516/2019/07/036

Clesse, S., & García-Bellido, J. 2017, Phys. Dark Univ., 15, 142, doi: 10.1016/j.dark.2016.10.002

—. 2022, Phys. Dark Univ., 38, 101111, doi: 10.1016/j.dark.2022.101111

Cotesta, R., Marsat, S., & Purrer, M. 2020, Phys. Rev. D, 101, doi: 10.1103/PhysRevD.101.124040

Cyr-Racine, F.-Y., & Sigurdson, K. 2013, Phys. Rev. D, 87, 103515, doi: 10.1103/PhysRevD.87.103515

Dal Canton, T., et al. 2014, Phys. Rev. D, 90, 082004, doi: 10.1103/PhysRevD.90.082004

D'Amico, G., Panci, P., Lupi, A., Bovino, S., & Silk, J. 2018, Mon. Not. Roy. Astron. Soc., 473, 328, doi: 10.1093/mnras/stx2419

Davies, G. S., Dent, T., Tápai, M., et al. 2020, Phys. Rev. D, 102, 022004, doi: 10.1103/PhysRevD.102.022004

Davies, G. S. C., & Harry, I. W. 2022, Class. Quant. Grav., 39, 215012, doi: 10.1088/1361-6382/ac8862

De Luca, V., Desjacques, V., Franciolini, G., Malhotra, A., & Riotto, A. 2019, JCAP, 05, 018, doi: 10.1088/1475-7516/2019/05/018

De Luca, V., Franciolini, G., Pani, P., & Riotto, A. 2020, JCAP, 04, 052, doi: 10.1088/1475-7516/2020/04/052

Essick, R., & Farr, W. 2022. https://arxiv.org/abs/2204.00461

Essick, R., Godwin, P., Hanna, C., Blackburn, L., & Katsavounidis, E. 2020, Machine Learning: Science and Technology, 2, 015004, doi: 10.1088/2632-2153/abab5f

Essick, R., et al. 2025, Phys. Rev. D, 112, 102001, doi: 10.1103/44x3-hv3y

Fairhurst, S., & Brady, P. 2008, Class. Quant. Grav., 25, 105002, doi: 10.1088/0264-9381/25/10/105002

Fisher, R. P., Hemming, G., Bizouard, M.-A., et al. 2020. https://arxiv.org/abs/2008.11316

Foreman-Mackey, D., Hogg, D. W., Lang, D., & Goodman, J. 2013, Publ. Astron. Soc. Pac., 125, 306, doi: 10.1086/670067

Ganapathy, D., Jia, W., Nakano, M., et al. 2023, Phys. Rev. X, 13, 041021, doi: 10.1103/PhysRevX.13.041021

García-Bellido, J. 2017, J. Phys. Conf. Ser., 840, 012032, doi: 10.1088/1742-6596/840/1/012032

Green, A. M., & Kavanagh, B. J. 2021, J. Phys. G, 48, 043001, doi: 10.1088/1361-6471/abc534

Gurian, J., Jeong, D., Ryan, M., & Shandera, S. 2022, Astrophys. J., 934, 121, doi: 10.3847/1538-4357/ac75e4

Hanna, C., et al. 2020, Phys. Rev. D, 101, 022003, doi: 10.1103/PhysRevD.101.022003

—. 2023, Phys. Rev. D, 108, 042003, doi: 10.1103/PhysRevD.108.042003

—. 2025, Phys. Rev. D, 112, 044013, doi: 10.1103/c97v-bmj8

Harris, C. R., et al. 2020, Nature, 585, 357, doi: 10.1038/s41586-020-2649-2

Harry, G. M., & the LIGO Scientific Collaboration. 2010, Classical and Quantum Gravity, 27, 084006, doi: 10.1088/0264-9381/27/8/084006

Hawking, S. 1971, Mon. Not. Roy. Astron. Soc., 152, 75, doi: 10.1093/mnras/152.1.75

Helmling-Cornell, A., Nguyen, P., Schofield, R., & Frey, R. 2024, Class. Quant. Grav., 41, 145003, doi: 10.1088/1361-6382/ad5139

Hunter, J. D. 2007, Comput. Sci. Eng., 9, 90, doi: 10.1109/MCSE.2007.55

Husa, S., Khan, S., Hannam, M., et al. 2016, Physical Review D, 93, 044006, doi: 10.1103/physrevd.93.044006

Hütsi, G., Raidal, M., Vaskonen, V., & Veermäe, H. 2021, JCAP, 03, 068, doi: 10.1088/1475-7516/2021/03/068

Huxford, R., George, R., Trevor, M., Yarbrough, Z., & Godwin, P. 2024. https://arxiv.org/abs/2412.04638

Isoyama, S., Sturani, R., & Nakano, H. 2020, doi: 10.1007/978-981-15-4702-7_31-1

Jia, W., et al. 2024, Science, 385, 1318, doi: 10.1126/science.ado8069

Joshi, P., et al. 2025a. https://arxiv.org/abs/2506.06497

—. 2025b. https://arxiv.org/abs/2505.23959

Kacanja, K., Soni, K., Akyüz, A., & Nitz, A. H. 2026. https://arxiv.org/abs/2602.12115

Kaplan, D. E., Krnjaic, G. Z., Rehermann, K. R., & Wells, C. M. 2011, JCAP, 10, 011, doi: 10.1088/1475-7516/2011/10/011

Khan, S., Husa, S., Hannam, M., et al. 2016, Physical Review D, 93, 044007, doi: 10.1103/physrevd.93.044007

LIGO–Virgo–KAGRA Collaboration. 2018, LVK Algorithm Library - LALSuite, Free software (GPL), doi: 10.7935/GT1W-FZ16

LIGO–Virgo–KAGRA Collaboration. 2026, Data Release for "Searches for Binary Mergers with Sub-solar Mass Components in Data from the First Part of LIGO–Virgo–KAGRA's Fourth Observing Run", Zenodo, doi: 10.5281/zenodo.19338460

LIGO Scientific Collaboration and Virgo Collaboration. 2018, Data quality report user documentation, docs.ligo.org/detchar/data-quality-report/

Macleod, D. M., Areeda, J. S., Coughlin, S. B., Massinger, T. J., & Urban, A. L. 2021, SoftwareX, 13, 100657, doi: 10.1016/j.softx.2021.100657

Magee, R., Deutsch, A.-S., McClincy, P., et al. 2018, Phys. Rev. D, 98, 103024, doi: 10.1103/PhysRevD.98.103024

Martynov, D. V., Hall, E. D., Abbott, B. P., et al. 2016, Phys. Rev. D, 93, 112004, doi: 10.1103/PhysRevD.93.112004

Messick, C., et al. 2017, Phys. Rev. D, 95, 042001, doi: 10.1103/PhysRevD.95.042001

Metzger, B. D., Hui, L., & Cantiello, M. 2024, Astrophys. J. Lett., 971, L34, doi: 10.3847/2041-8213/ad6990

Mohapatra, R. N., & Teplitz, V. L. 1999, Phys. Lett. B, 462, 302, doi: 10.1016/S0370-2693(99)00789-3

Mozzon, S., Nuttall, L. K., Lundgren, A., et al. 2020, Class. Quant. Grav., 37, 215014, doi: 10.1088/1361-6382/abac6c

Nakamura, T., Sasaki, M., Tanaka, T., & Thorne, K. S. 1997, Astrophys. J. Lett., 487, L139, doi: 10.1086/310886

Ng, K. K. Y., Franciolini, G., Berti, E., et al. 2022, Astrophys. J. Lett., 933, L41, doi: 10.3847/2041-8213/ac7aae

Ng, K. K. Y., et al. 2023, Phys. Rev. D, 107, 024041, doi: 10.1103/PhysRevD.107.024041

Nitz, A., et al. 2024, gwastro/pycbc: v2.3.3 release of PyCBC, v2.3.3, Zenodo, doi: 10.5281/zenodo.10473621

Nitz, A. H., Capano, C., Nielsen, A. B., et al. 2019, Astrophys. J., 872, 195, doi: 10.3847/1538-4357/ab0108

Nitz, A. H., Dent, T., Dal Canton, T., Fairhurst, S., & Brown, D. A. 2017, Astrophys. J., 849, 118, doi: 10.3847/1538-4357/aa8f50

Nitz, A. H., & Wang, Y.-F. 2021a, Astrophys. J., 915, 54, doi: 10.3847/1538-4357/ac01d9

—. 2021b, Phys. Rev. Lett., 126, 021103, doi: 10.1103/PhysRevLett.126.021103

Owen, B. J. 1996, Phys. Rev. D, 53, 6749, doi: 10.1103/PhysRevD.53.6749

Pan, Y., Buonanno, A., Baker, J. G., et al. 2008, Phys. Rev. D, 77, doi: 10.1103/PhysRevD.77.024014

pandas development team, T. 2024, pandas-dev/pandas: Pandas, v2.2.0, Zenodo, doi: 10.5281/zenodo.10537285

Peters, P. C., & Mathews, J. 1963, Phys. Rev., 131, 435, doi: 10.1103/PhysRev.131.435

Phukon, K. S., Baltus, G., Caudill, S., et al. 2021. https://arxiv.org/abs/2105.11449

Pratten, G., et al. 2021, Phys. Rev. D, 103, 104056, doi: 10.1103/PhysRevD.103.104056

Radice, D., Perego, A., Zappa, F., & Bernuzzi, S. 2018, Astrophys. J. Lett., 852, L29, doi: 10.3847/2041-8213/aaa402

Raidal, M., Spethmann, C., Vaskonen, V., & Veermäe, H. 2019, JCAP, 02, 018, doi: 10.1088/1475-7516/2019/02/018

Ray, A., et al. 2023. https://arxiv.org/abs/2306.07190

Robinet, F., Arnaud, N., Leroy, N., et al. 2020, SoftwareX, 12, 100620, doi: 10.1016/j.softx.2020.100620

Rosenberg, E., & Fan, J. 2017, Phys. Rev. D, 96, 123001, doi: 10.1103/PhysRevD.96.123001

Ryan, M., Gurian, J., Shandera, S., & Jeong, D. 2022a, Astrophys. J., 934, 120, doi: 10.3847/1538-4357/ac75ef

Ryan, M., Shandera, S., Gurian, J., & Jeong, D. 2022b, Astrophys. J., 934, 122, doi: 10.3847/1538-4357/ac75e5

Sachdev, S., et al. 2019. https://arxiv.org/abs/1901.08580

Sakon, S., et al. 2024, Phys. Rev. D, 109, 044066, doi: 10.1103/PhysRevD.109.044066

Sasaki, M., Suyama, T., Tanaka, T., & Yokoyama, S. 2016, Phys. Rev. Lett., 117, 061101, doi: 10.1103/PhysRevLett.117.061101

Servignat, G., Davis, P. J., Novak, J., Oertel, M., & Pons, J. A. 2024, Phys. Rev. D, 109, 103022, doi: 10.1103/PhysRevD.109.103022

Shandera, S., Jeong, D., & Gebhardt, H. S. G. 2018, Phys. Rev. Lett., 120, 241102, doi: 10.1103/PhysRevLett.120.241102

Siles, J. F. N., & García-Bellido Capdevila, J. 2025, Phys. Dark Univ., 47, 101789, doi: 10.1016/j.dark.2024.101789

Singh, D. 2024, PhD thesis, Penn State U., Penn State U.

Singh, D., Ryan, M., Magee, R., et al. 2021, Phys. Rev. D, 104, 044015, doi: 10.1103/PhysRevD.104.044015

Smith, J. R., Abbott, T., Hirose, E., et al. 2011, Class. Quant. Grav., 28, 235005, doi: 10.1088/0264-9381/28/23/235005

Soni, S., Berger, B. K., Davis, D., et al. 2025, Classical and Quantum Gravity, 42, 085016, doi: 10.1088/1361-6382/adc4b6

Stovall, K., et al. 2018, Astrophys. J. Lett., 854, L22, doi: 10.3847/2041-8213/aaad06

Talbot, C., Farah, A., Galaudage, S., Golomb, J., & Tong, H. 2025, Journal of Open Source Software, 10, 7753, doi: 10.21105/joss.07753

Tsukada, L., et al. 2023, Phys. Rev. D, 108, 043004, doi: 10.1103/PhysRevD.108.043004

Urban, A. L., et al. 2021, gwdetchar/gwdetchar, doi.org/10.5281/zenodo.2575786, Zenodo, doi: 10.5281/zenodo.597016

Usman, S. A., et al. 2016, Class. Quant. Grav., 33, 215004, doi: 10.1088/0264-9381/33/21/215004

Vaskonen, V., & Veermäe, H. 2020, Phys. Rev. D, 101, 043015, doi: 10.1103/PhysRevD.101.043015

Viets, A., et al. 2018, Class. Quant. Grav., 35, 095015, doi: 10.1088/1361-6382/aab658

Virgo Collaboration. 2021, PythonVirgoTools, v5.1.1, git.ligo.org/virgo/virgoapp/PythonVirgoTools

Virtanen, P., et al. 2020, Nature Meth., 17, 261, doi: 10.1038/s41592-019-0686-2

Waskom, M. 2021, J. Open Source Softw., 6, doi: 10.21105/joss.03021

1903 Wette, K. 2020, SoftwareX, 12, 100634,
1904 doi: 10.1016/j.softx.2020.100634

1905 Zweizig, J. 2006, The Data Monitor Tool Project,
1906 labcit.ligo.caltech.edu/~jzweizig/DMT-Project.html